Renewable and Sustainable Energy Reviews 45 (2015) 296–317

Contents lists available at ScienceDirect

Renewable and Sustainable Energy Reviews

journal homepage: www.elsevier.com/locate/rser

Two-phase flow pressure drop in flow channels of proton exchange membrane fuel cells: Review of experimental approaches

Mehdi Mortazavi*, Kazuya Tajiri

Mechanical Engineering-Engineering Mechanics, Michigan Technological University, 1400 Townsend Drive, Houghton, MI 49931, United States

ARTICLE INFO

Article history:
Received 3 April 2014
Received in revised form
22 September 2014
Accepted 7 January 2015

Keywords:
Proton exchange membrane (PEM) fuel cell
Two-phase flow pressure drop
PEM fuel cell flow channels

ABSTRACT

Water management in proton exchange membrane (PEM) fuel cells has stimulated an extensive research on different aspects of water transport phenomena. As a PEM fuel cell operates, power is produced with water and heat as inevitable byproducts. The water produced during the operation of a PEM fuel cell results in a liquid–gas two-phase flow in flow channels. A successful PEM fuel cell design requires a comprehensive knowledge about different properties of liquid–gas two-phase flow. One such property, that has a dominant impact on the performance of a PEM fuel cell, is the two-phase flow pressure drop within the flow channels. This paper reviews the two-phase flow pressure drop correlations that have been developed for the application of PEM fuel cell. It also reviews the effect of different working conditions on the two-phase flow pressure drop in PEM fuel cell flow channels.

Contents

1. Introduction

A proton exchange membrane (PEM) fuel cell is considered to be an efficient and pollutant free energy system that can generate

* Corresponding author.
E-mail addresses: mortazav@mtu.edu (M. Mortazavi), ktajiri@mtu.edu (K. Tajiri).

http://dx.doi.org/10.1016/j.rser.2015.01.044
1364-0321/

Nomenclature

[Bo] Bond number
[$Bo^{\star}$] modified Bond number
[C] parameter in Lockhart–Martinelli correlation
[D] channel diameter
[D_h] hydraulic diameter
[Fr] Froude number
[f] Fanning friction factor
[g] gravitational acceleration
[G] mass flux (kg/m^2 s)
[j_f] superficial liquid velocity
[j_g] superficial gas velocity
[N_{conf}] confinement number
[P] pressure
[P_c] critical pressure
[Re] Reynolds number
[Re_f] Reynolds number based on superficial liquid velocity, $Re_f = G(1-x)D_h/\mu_f$
[v] specific volume
[We] Weber number
[x] mass flow quality, coordinate
[X] Lockhart–Martinelli parameter

Greek symbols

[Δ] difference
[α] void fraction
[ρ] density
[β] channel aspect ratio ($\beta < 1$)
[σ] surface tension
[ϕ] two-phase flow frictional multiplier, channel inclination angle
[μ] dynamic viscosity

Subscript

[A] acceleration
[F] frictional
[G] gravitational
[TP] two-phase
[f] saturated liquid
[g] saturated vapor
[z] stream wise coordinate
[fg] difference between saturated vapor and saturated liquid
[fo] liquid only
[go] vapor only
[tt] turbulent liquid–turbulent vapor
[tv] turbulent liquid–laminar vapor
[vt] laminar liquid–turbulent vapor
[vv] laminar liquid–laminar vapor

power for various applications [1,2]. The electrochemical reactions within the electrodes utilize hydrogen and oxygen to generate electricity with heat and water as the byproducts. Reliable fuel cell performance, however, hinges upon a uniform and continuous supply of reactants across the electrodes. The water produced during the operation of the cell can fill open pores of the gas diffusion layer (GDL) and block the transport of the reactants to the catalyst layers. This phenomenon is referred to as GDL flooding and has been reported to extensively deteriorate the performance of the cell [3–5]. Accumulated liquid water within the GDL emerges from its surface at some preferential locations [6]. The liquid water that emerged from the surface of the GDL can be removed by different mechanisms, depending on the gas flow rate and water production rate [7]. When the water removal rate is less than the water production rate, a water lens may form within the gas channel. The growth of this lens can ultimately clog the gas channel and block the transport of the reactants to the catalyst layer. This phenomenon is referred to as channel flooding and similar to GDL flooding, it can lower the overall performance of the cell [8–10]. A uniform and continuous supply of reactants across the electrodes can be achieved by acquiring an accurate understanding about the liquid water behavior within the GDL and gas channel.

The accumulation of liquid water within the gas channel follows with the formation of a two-phase flow during the operation of the cell. Channel flooding becomes even more discernible at low temperatures and/or high current densities in which water accumulation increases because of water condensation and water production, respectively.

The transport of an elongated water slug within the gas channel may be influenced by three forces of gravity, surface tension, and shear force of the core gas flow. Bond number, $Bo = (\rho_f - \rho_g)gD^2/\sigma$, describes the ratio of the gravity force to the surface tension effect. The small characteristic length scale associated with the PEM fuel cell suggests that gravity's impact on the two-phase flow is insignificant while surface tension has a dominant impact. Moreover, the small characteristic length scales suggest that capillary forces are important to the behavior of liquid surfaces.

Different methods of studying the two-phase flow in gas channels can be categorized as direct and indirect techniques. Direct techniques include monitoring the liquid–gas flow within the gas channel either through a transparent cell [7,10–15], neutron imaging [16,17], X-ray microtomography [18,19], or gas chromatography [20,21]. Bazylak comprehensively reviewed different methods of visualizing liquid water in PEM fuel cell flow fields [22].

The indirect study of the liquid–gas two phase flow in PEM fuel cells can be accomplished by measuring the parameters that are the immediate result of the liquid water accumulation. One such parameter can be the two-phase flow pressure drop along the gas channel as the accumulated water resists the gas flow and causes an increase in the pressure drop. Thus, the two-phase flow pressure drop can be considered as an in situ diagnostic tool that can reveal information about the amount of liquid water accumulated within the gas channel. While a low pressure drop along the flow channel is desired because of the lower compressor power to supply reactant gases, a minimum pressure drop along the gas channel should be maintained to ensure condensate removal from the flow channels. Different aspects of liquid–gas two-phase flow in gas flow channels of PEM fuel cells have been reviewed by Anderson et al. [23].

In this paper, the two-phase flow pressure drop in the PEM fuel cell flow channels is reviewed. This is achieved first by reviewing the two-phase flow patterns and two-phase flow pressure drop models proposed for general applications. The study is then followed by focusing on the two-phase flow pressure drop with the application of PEM fuel cells. In Section 2, different patterns of two phase flows are introduced. The models developed to predict the two-phase flow pressure drop are presented in Section 3. Section 4 focuses on the two-phase flow pressure drop in PEM fuel

cells. In Section 5 the models that have been proposed for predicting the two-phase flow pressure drop in PEM fuel cell flow channels are reviewed. The overall conclusions drawn from this study are presented in Section 6. It should be added that only literature with experimental approaches are reviewed in this paper and studies with computational approaches are not included.

2. Two-phase flow

Liquid–gas two phase flow is a common type of flow in many industrial applications such as heat exchangers, condensers, chemical processing plants, air conditioners, and fuel cells. Two phase flow occurs in different patterns depending on the liquid to gas ratio, the superficial velocity of each phase, the surface characteristics of the channel, and the channel geometry. The superficial fluid velocity is defined as the bulk velocity of the fluid flowing within the channel cross-sectional area. In this section, different two phase flow patterns introduced in literature are reviewed. All of the flow patterns observed both in general application and PEM fuel cell will be introduced. The section starts with presenting the channel classification considered in this paper. The classification has been proposed by Kandlikar [24] and can be considered to be a sound reference for categorizing small flow channels with engineering applications. After reviewing different patterns of two-phase flow, liquid water transport mechanisms through and on the surface of the GDL will be introduced.

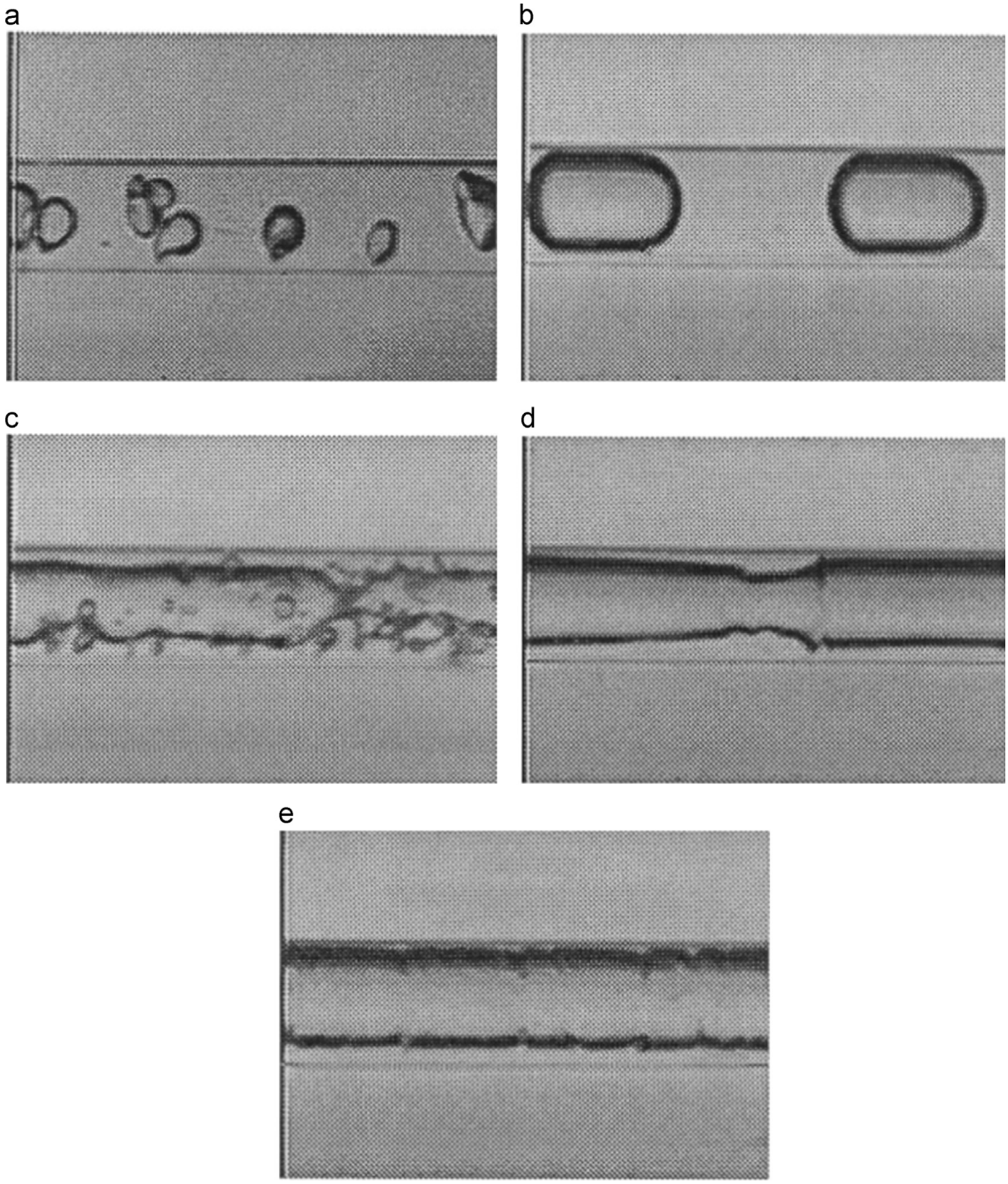

Fig. 1. Two phase flow patterns reported by Triplett et al. [25]. (a) Bubbly flow $j_f = 3.021$ m/s, $j_g = 0.083$ m/s. (b) Slug flow $j_f = 0.213$ m/s, $j_g = 0.154$ m/s. (c) Churn flow $j_f = 1.205$ m/s, $j_g = 4.631$ m/s. (d) Slug-annular flow $j_f = 0.043$ m/s, $j_g = 4.040$ m/s. (e) Annular flow $j_f = 0.082$ m/s, $j_g = 73.30$ m/s.

2.1. Channel classification

Two-phase flow occurs in many engineering applications with different length scales. The length scale of a channel defines the forces that can affect the transport mechanism. For instance, the two phase flow in small channels of a compact heat exchanger is significantly affected by the surface characteristics, while the effects of surface characteristics on the two-phase flow passing through a large pipe of a chemical processing plant are almost negligible. An accurate study of the two-phase flow can only be accomplished by assorting flows based on their channel size. Kandlikar [24] has proposed a channel classification that can be used both for single phase and two-phase flows. The proposed classification is based on the channel hydraulic diameter and spans from sub-microns to millimeters. According to the classification proposed, channels with hydraulic diameters greater than 3 mm are referred to as conventional channels. Fuel cell gas channels are categorized as minichannels with hydraulic diameters between 200 μm and 3 mm. The classification considers channels with hydraulic diameters between 10 μm and 200 μm as microchannels. However, microchannels fall below the length scale of PEM fuel cell gas channels.

2.2. Two-phase flow patterns

Different patterns of two-phase flow in minichannels have been well categorized by Triplett et al. [25]. They supplied water and air through circular and semi-triangular (with one corner smoothed) minichannels of Pyrex with different hydraulic diameters between 1.09 mm and 1.49 mm. According to their classification, the two phase flow in minichannels can transport in five different patterns, bubbly flow, slug flow, churn flow, slug-annular flow, and annular flow, as shown in Fig. 1. Bubbly flow contains randomly dispersed bubbles with diameters smaller than the channel diameter. Slug flow includes elongated bubbles and occurs at a lower superficial liquid velocity compared to bubbly flow. Bubbles can elongate by increasing the superficial gas velocity and/or decreasing the superficial liquid velocity. Churn flow is characterized by unstable bubbles or wavy annular flow and transits into slug-annular flow at lower liquid flow rates. The slug-annular flow can be described as wavy-annular flow with individual waves that do not block the channel. Finally, a dramatic increase in the superficial gas velocity eliminates the wavy form of the slug-annular flow and results in annular flow within the gas channel.

Two-phase flow patterns have been extensively studied in other literature [26–40]. Two-phase flow patterns are not limited to the patterns that have been defined by Triplett et al. [25] in minichannels. For instance in conventional channels, Wambsganss et al. [34] have defined stratified flow pattern as having a smooth liquid and gas interface. In this pattern of two-phase flow, liquid flows on the bottom of the channel because of the gravity. However, it should be mentioned that the two-phase flow patterns introduced by Triplett et al. [25] are the main flow patterns that can be observed in mini-channels.

Zhao and Bi [41] reported that each pattern of two-phase flow has its own pressure drop profile signature. The bubbly flow, for instance, has minimal pressure drop with the least pressure oscillation. Annular flow, on the other hand, is reported to have the maximum pressure drop with moderate pressure oscillation. The high pressure drop in annular flow originates from the high gas flow rate. Finally, the maximum pressure oscillation is mentioned to occur in churn flow.

Not all of the flow patterns that have been introduced by Triplett et al. [42] occur in PEM fuel cell flow channels. For instance, the low superficial liquid velocity in PEM fuel cell gas channels does not allow the formation of bubbly flow. The superficial water velocity in PEM fuel cell channels is defined based on water production rate which itself is a function of current density. Similarly, the formation of churn flow is impossible as it requires a high liquid to gas ratio. Water transport in the gas channels of PEM fuel cells has been studied and categorized by Zhang et al. [7]. They studied water transport in gas flow channels of a transparent PEM fuel cell and observed that flow patterns change with superficial gas velocity and the liquid water production rate. For a low water production rate and a low gas flow rate, water can spread over hydrophilic channels and drain via channel corners. When the water production rate is moderate and corner flow is not sufficient to remove liquid water with a comparable rate, corner flow may change into annular film flow within the gas channel. The instability of thick water films may turn the annular film flow into slug flow which eventually clogs the channel and shuts off the cell. Fig. 2 shows the three flow patterns of corner flow, annular film flow, and slug flow reported by Zhang et al. [7]. Other than these, another pattern of two-phase flow has also been classified which is the characteristic of high gas flow rates. For sufficiently high gas flow rates, the shear force of the core gas flow can detach water droplets from the GDL surface to form mist flow.

The two phase flow map at different liquid and gas flow ranges has been investigated in many studies [10,25–27,29,41,43–48]. Lu et al. [44] presented a flow pattern map for flow ranges of PEM fuel cells, as shown in Fig. 3. The map contains different flow patterns that have been identified by Zhang et al. [7] The flow pattern map shown in Fig. 3 can be used to determine the water

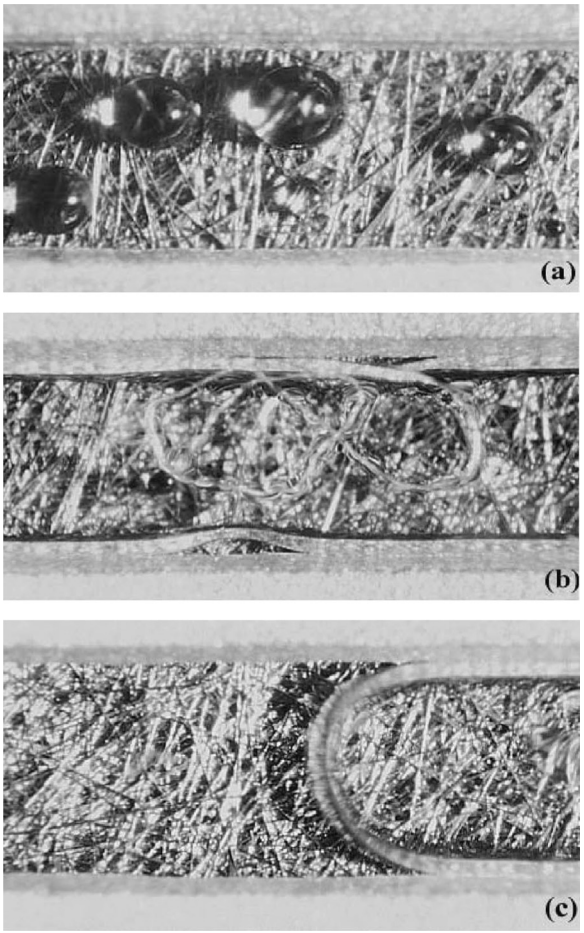

Fig. 2. Two phase flow patterns observed in PEM flow channels reported by Zhang et al. [7]. (a) Corner flow, (b) annular film flow, (c) slug flow.

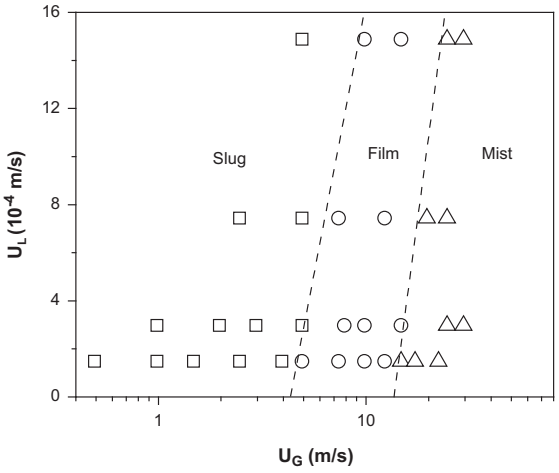

Fig. 3. Two-phase flow pattern map reported by Lu et al. [44].

transport mechanism at different water and air superficial velocities.

Among different two phase flow patterns that occur in PEM fuel cell flow channels, mist flow is reported to be the most efficient mode of liquid water removal from the gas channels [44]. However, its high pressure drop requirements lowers the overall efficiency of the system. Despite mist flow that requires a high pressure drop, slug flow occurs at low pressure drop but this pattern of two-phase flow is not desirable as it can lead to performance degradation because of its low water removal rate [44]. Moreover, slug flow may also lead to flow mal-distribution that is defined as the accumulation of excess water in one channel while other channels dry out because of excessive air flow rate [49]. Flow mal-distribution has been reported to reduce the operating lifetime of a fuel cell [50]. While mist flow and slug flow are not suitable modes of liquid water transport in PEM fuel cell flow channels, film flow has been reported to be a desirable mode of liquid water removal as it can be achieved at a moderate pressure drop and is capable of keeping an appropriate balance between the produced water and the removed water [44]. Furthermore, film flow is reported to be a desirable liquid water transport mode in PEM fuel cells because water transports along the channel sidewalls instead of the GDL surface [51].

Because slug flow is the most common flow pattern in PEM fuel cells [44], more attention should be paid to eliminate the issues that arise with this pattern of flow. One such issue can be the flow mal-distribution with the direct consequences being current re-distribution, erratic current fluctuation, and pressure drop fluctuation within the cell. Flow mal-distribution in PEM fuel cell parallel gas channels has been extensively investigated [49,52–54]. The overall conclusion suggests that the equal pressure drop for multiple parallel gas channels does not necessarily ensure even distribution of gas and liquid phases. This is because different combinations of liquid and gas flow rates can result in the same pressure drop.

2.3. Liquid water transport through the porous GDL

In Section 2.2, different modes of liquid water transport in gas channels of the PEM fuel cell were reviewed. While researchers have acquired a solid knowledge about water transport mechanisms within the gas channels of the PEM fuel cell, water transport mechanisms through the porous structure of GDL is still under discussion. In this section, some major hypotheses about water transport mechanisms through the GDL will be introduced.

Nam and Kaviany [55] investigated the distribution of condensed water within the GDL and suggested that the liquid water is transported from the catalyst layer to the gas channel in a branching type geometry. Based on their model, micro-droplets form in the condensation site of the catalyst layer and are transported into the larger pores of the GDL, via capillary flow, to form macro-droplets. The capillary transport continues until a large droplet emerges from the surface of the GDL. This transport mechanism can be described as tree-like percolation and has been confirmed by Pasaogullari and Wang [5].

Benziger et al. [56] modeled GDL as a single solid layer which contains parallel microchannels with different diameters. Liquid water passes through the channel with the largest diameter to yield the minimum breakthrough pressure.

Litster et al. [57] employed fluorescence microscopy to visualize the water transport through the GDL. They postulated that water transport is mostly dominated by fingering and channeling and does not necessarily follow the capillary tree model suggested in [5,55]. Bazylak et al. [6] followed the same visualization technique and observed that droplets emerge from the surface of the GDL at preferential locations. These locations were reported to randomly change over time. According to their observation, the GDL was described as a network of pores that is characterized by dynamic interconnections of water pathways.

Tamayol and Bahrami [58] modeled the GDL as a network of pores connected by throats. The throats resist the water transport through the GDL while pores do not apply any resistance. The GDL model proposed by Tamayol and Bahrami [58] confirms the transport behavior observed by Bazylak [6].

Different models of liquid water transport through the GDL were reviewed. The tortuous structure of the GDL may justify the possibility of each of these mechanisms. The results reported in an in situ study done with synchrotron X-ray radiography [59] confirms the dynamic transport model proposed by Litster [57] and Bazylak [22] as well as the branching-type geometry proposed by Pasaogullari and Wang [5] and Nam and Kaviany [55].

3. Two-phase flow pressure drop models

The single-phase pressure drop in fluids is well understood and can be predicted over a wide range of operating conditions. The liquid–gas two-phase flow pressure drop, however, is not well identified and has been studied only for a limited range of operating conditions relevant to particular areas of interest. The physics behind this type of transport phenomena is very complicated to be modeled with simplified mathematical expressions. Therefore, the majority of published works try to improve the already known expressions by correlating the experimental results.

The two-phase flow pressure drop is the sum of frictional, gravitational and accelerational pressure drop:

$$\Delta P_{TP} = \Delta P_{TP,F} + \Delta P_{TP,G} + \Delta P_{TP,A} \tag{1}$$

The acceleration pressure gradient is expressed as

$$-\left(\frac{dP}{dz}\right)_A = G^2 \frac{d}{dz}\left[\frac{v_g x^2}{\alpha} + \frac{v_f (1-x)^2}{(1-\alpha)}\right] \tag{2}$$

where mass flow quality, x, is defined as

$$x = \frac{G_g}{G_g + G_f} \tag{3}$$

The void fraction α is the gas hold-up in the liquid stream and can be measured by different methods, such as constant electric current method [60], quick closing valve [26], and even image analysis [29,28]. Zivi [61] expressed void fraction as a function of

Table 1
Literature comparing the predicted and measured two-phase flow pressure drops.

Author	Channel geometry[1]	Channel material	D_h (mm)	Fluids	Mass flux kg m^{-2} s^{-1}
Bao et al. [65]	C, UV, H	Glass and copper	Glass (0.74–3.07) Copper (1.98)	Air–water Glycerin water mixture	Water 7–2400 Air 0.18–60
Chang and Ro [66]	C, H	Copper	1.2, 1.6	Pure R-32, R-125, R-134A and their mixture	3980–9370
Yan and Lin [67]	C, H	Not Specified	2	R-134A	50–200
Wang et al. [38]	C, H	Copper	3.17	Air–water	50–700
Wang et al. [68]	C, H	Not Specified	3–9	R-22, R-407C, R-410A	50–700
Zhao and Bi [41]	T, UV	Lucite	0.886–2.886	Air–water	water 10–10,000 Air 0.12–120
Chen et al. [69]	C, H	Copper	Air–water (1.02–7.02) R-410A (3.17–9)	Air–water R-410A	Air–water (50–3000) R-410A (50–600)
Zhang and Webb [70]	C, H	Aluminum, copper	Al (2.13) Copper (3.25, 6.25)	R-134A, R-22, R-404A	200–1000
Kawahara et al. [28]	C, H	Fused silica	0.1	De-ionized water–nitrogen	Water 20–4000 Nitrogen 0.12–72
Yu et al. [71]	C, H	Stainless steel	2.98	Water, ethylene glycol and mixture	50–200
Bandarra Filho et al. [72]	C, H	Copper	6.24–8.92	R-134A	70–1100
Greco and Vanoli [73]	C, H	Stainless steel	6	R-22, R-507	250–286
Wongsa-ngam et al. [74]	C, H	Copper	8.12	R-134A	400–800
Choi and Pamitran [75]	C, H	Stainless steel	1.5, 3	R-410A, R-407C	300–600
Wongwises and Pipathattakul [26]	C, H, inclined (30°, 60°)	Acrylic glass	8	Air–water	Water 69–6020 Air 0.026–78.6
Pehlivan et al. [76]	C, H	Borosilicate glass	0.8–3	Air–water	Water 20–1000 Air 12–120
Chen et al. [77]	R, H	Transparent acrylic resin	3–5	Air–water	100–700
Mauro et al. [78]	C, H	Stainless steel	6	R-22, R-134A, R-404A, R-407C R-410A, R-417A, R-507A	190–1150
Lee and Lee [79]	C, H	Teflon, Glass, polyurethane	1.62–2.16	Air–water	Water 6–154 Air 0.05–0.65
Saisorn and Wongwises [27]	C, H	Fused silica	0.53	Air–water	Water 5–3040 Air 0.44–19.2
Choi et al. [62]	C, H	Stainless steel	1.5, 3	R-410A	300–600
Tran et al. [80]	C, R, H	Brass (R-134A, R-12) Stainless steel (R-113)	C (2.46, 2.92) R (2.39)	R-134A, R-12, R-113	R-134A 33-502 R-12 44-832 R-113 50-400
da Silva Lima et al. [81]	C, H	Stainless steel	14	R-717 (ammonia)	50-160
Hu et al. [82]	C, H	Not specified	2, 4.18	R-410A, oil	200–620
Kaew-On and Wongwises [83]	R, H	Aluminum	3.48	R-410A	200–400
Quiben et al. [84]	C, flattened, H	Copper	C (8–13.84) Flattened (3.71–5.35)	R-22, R-410A	150–500
Choi et al. [37]	R, H	Photosensitive glass	0.143–0.49	Water–nitrogen gas	Liquid 66–1000 Gas 0.07-80
Venkatesan et al. [36]	C, H	Silica glass	0.6–3.4	Air–water	Water 10–3000 Gas 0.01–60
Wu et al. [85]	C, H	Stainless steel	1.42	CO_2	300–600
Saisorn and Wongwises [86]	C, H	Fused silica	0.15, 0.53	Air–water	Not specified

C: circular, R: rectangular, T: triangular, UV: upward vertical, H: horizontal.

mass flow quality, x, and liquid and gas density:

$$\alpha = \left[1 + \left(\frac{1-x}{x}\right)\left(\frac{\rho_g}{\rho_f}\right)^{2/3}\right]^{-1} \quad (4)$$

It has been shown that for low liquid and gas superficial velocities, the acceleration pressure drop incorporates a small fraction of the overall two-phase flow pressure drop [42], while the acceleration pressure drop becomes significant at high superficial velocities [42,62].

For an inclined channel with the inclination angle of ϕ, the gravitational pressure gradient can be expressed as

$$-\left(\frac{dP}{dz}\right)_G = [\alpha\rho_g + (1-\alpha)\rho_f]g \sin\phi \quad (5)$$

For a horizontal channel, this angle will equal zero and the overall gravitational pressure gradient will be zero. Gravitational pressure gradient has a significant contribution to the overall

Table 2
Two-phase viscosity model.

Author	Equation
McAdams et al. [87]	$\frac{1}{\mu_{TP}} = \frac{x}{\mu_g} + \frac{1-x}{\mu_f}$
Akers et al. [88]	$\mu_{TP} = \frac{\mu_f}{\left[(1-x) + x\left(\frac{\nu_g}{\nu_f}\right)^{0.5}\right]}$
Cicchitti et al. [89]	$\mu_{TP} = x\mu_g + (1-x)\mu_f$
Owens [90]	$\mu_{TP} = \mu_f$
Dukler et al. [91]	$\mu_{TP} = \frac{x\nu_g\mu_g + (1-x)\nu_f\mu_f}{x\nu_g + (1-x)\nu_f}$
Beattie and Walley [92]	$\mu_{TP} = \beta\mu_g + (1-\beta)(1+2.5\beta)\mu_f$ $\beta = \frac{\rho_f x}{\rho_f x + \rho_g(1-x)}$ (here β is not the aspect ratio)
Lin et al. [93]	$\mu_{TP} = \frac{\mu_f\mu_g}{\mu_g + x^{1.4}(\mu_f - \mu_g)}$

pressure drop in macro-channels and becomes even more dominant in low mass velocities. For mini/micro channels, however, the dominant impact of surface tension diminishes the gravitational effects.

The two-phase flow frictional pressure drop is generally predicted based on two different approaches, depending on how each phase of fluid is treated. In one approach, the two-phase mixture is considered as a pseudo single phase fluid with properties such as viscosity and density weighted to the quality. This model is known as the homogeneous equilibrium model (also referred to as the viscosity model) and has been proven to give a more accurate prediction at higher mass qualities [33,47,63]. In the other method, the two-phase pressure drop corresponds to the single-phase pressure drop multiplied by a two-phase flow frictional multiplier, ϕ. This method is known as the separated flow model and was originally introduced by Lockhart and Martinelli in 1949 [64].

Much research has been done to compare the experimentally measured frictional two-phase flow pressure drops with those predicted by homogeneous and/or separated flow models. Table 1 lists some studies doing such comparisons.

3.1. Homogeneous equilibrium model

In the homogeneous equilibrium model the two-phase mixture is treated as a pseudo single-phase fluid and the properties are mean weighted relative to each liquid and gas content. Because it is assumed that the liquid and gas phases are moving at the same speed, this model has also been named the zero slip model. According to the homogeneous method, the two-phase flow pressure drop can be calculated by

$$\left(\frac{dP}{dz}\right)_{TP}=\frac{2f_{TP}G^2}{D_h\rho_{TP}} \tag{6}$$

where the two-phase friction factor, f_{TP}, depends on the two-phase flow Reynolds number, Re_{TP}:

$$f_{TP}=\begin{cases}\dfrac{16}{Re_{TP}} & \text{for } Re_{TP}<2000\\ 0.079Re_{TP}^{-0.25} & \text{for } 2000\le Re_{TP}<20,000\\ 0.046Re_{TP}^{-0.2} & \text{for } Re_{TP}\ge 20,000\end{cases} \tag{7}$$

The two-phase Reynolds number is calculated based on the two-phase mixture viscosity, μ_{TP}:

$$Re_{TP}=\frac{GD_h}{\mu_{TP}} \tag{8}$$

Different models of two-phase viscosity have been introduced [87–93] and are well discussed and compared [94–97]. Table 2 lists some of the two-phase viscosity models that have been introduced.

In Eq. (6), ρ_{TP} is the density of the pseudo fluid and is given by

$$\rho_{TP}=\left(\frac{x}{\rho_g}+\frac{1-x}{\rho_f}\right)^{-1} \tag{9}$$

For rectangular channels and for laminar flow, the two-phase friction factor, f_{TP}, can also be obtained by [98]

$$f_{TP}Re_{TP}=24[1-1.3553\beta+1.9467\beta^2-1.7012\beta^3+0.9564\beta^4-0.2537\beta^5] \tag{10}$$

where β is the aspect ratio of the channel and is defined as the ratio of the width to the height of the channel.

The accuracy of the homogeneous flow model in predicting the two-phase flow pressure drop was examined by Triplett et al. [42]. It has been reported that although the homogeneous flow model can appropriately predict the pressure drop for bubbly and slug flows, it results in significant deviation from the actual pressure drop in slug-annular and annular flow patterns. Even at a low Reynolds number, such as 70, the homogeneous flow model was observed to over-predict the pressure drop.

3.2. Separated flow model

In the separated flow model, the two-phase flow pressure drop is predicted based on the pressure drop of one phase multiplied by the two-phase frictional multiplier:

$$\left(\frac{dP}{dz}\right)_{TP}=\phi_f^2\left(\frac{dP}{dz}\right)_f \tag{11}$$

where ϕ_f^2 is the two-phase frictional multiplier based on liquid and has been reported to depend on the flow pattern [99]. The Martinelli parameter, X, is defined as

$$X=\left[\left(\frac{dP}{dz}\right)_f\Big/\left(\frac{dP}{dz}\right)_g\right]^{1/2} \tag{12}$$

This model was followed by Chisholm [100] by introducing the Chisholm parameter, C. The Chisholm parameter is used to define the frictional multiplier:

$$\phi_f^2=\frac{\left(\frac{dP}{dz}\right)_{TP}}{\left(\frac{dP}{dz}\right)_f}=1+\frac{C}{X}+\frac{1}{X^2} \tag{13}$$

The original concept of the Chisholm correlation (Eq. (13)) came from the fact that the two-phase flow pressure drop is equal to the sum of the pressure drop for each of the phases of liquid and gas and the interaction between these two phases:

$$\left(-\frac{dp}{dz}\right)_{TP}=\left(-\frac{dp}{dz}\right)_f+\left(-\frac{dp}{dz}\right)_g+C\left[\left(-\frac{dp}{dz}\right)_f\left(-\frac{dp}{dz}\right)_g\right]^{1/2} \tag{14}$$

The Chisholm parameter, C, is a measure of the interaction between two phases, and similar to the frictional multiplier, it has been reported to depend on the flow regime [99]. Table 3 lists the values of the Chisholm parameters depending on the flow regimes of liquid and gas phases [100].

Many studies have investigated the two-phase flow pressure drop for different applications based on the separated flow model. Table 4 lists some of the proposed pressure drop correlations based on the separated flow model.

Friedel [101] used 25,000 data points of pressure drops in horizontal pipes with diameters greater than 44 mm and correlated ϕ_f^2 with gravity, surface tension, and total mass flux using Froud and Weber numbers, as given in Table 4.

Müller-Steinhagen and Heck [102] proposed a new correlation for the two-phase flow frictional pressure drop by considering 9300 data points for different fluids passing through the channels with diameters ranging from 4 mm to 392 mm. Their correlation has been known as a reliable frictional pressure drop model that provides minimal deviation from the actual pressure drop compared to other existing correlations [29,94,103,104].

Most of the early studies done on the two-phase flow pressure drop were based on the pressure drop measured in channels with

Table 3
Values of Chisholm parameter [100].

Two-phase flow characteristics	Chisholm's parameter C
Laminar liquid–laminar gas	5
Turbulent liquid–laminar gas	10
Laminar liquid–turbulent gas	12
Turbulent liquid–turbulent gas	21

large hydraulic diameters. The correlations proposed in those studies proved to yield an inferior prediction of pressure drop in recently developed micro-scale devices. As the channel size decreases from conventional channel to mini-/micro-channels, the surface tension effects become more dominant and the gravity becomes less important. Most of the studies focusing on the two-phase flow pressure drop in mini/micro channels concentrate on a specific application such as compact heat exchangers, refrigeration systems, or microtube condensers.

Lowry and Kawaji [35] were among the first researchers who studied the two-phase flow pressure drop in minichannels. They investigated the variation of ϕ^2 with dimensionless gas velocity and concluded that although the two-phase frictional multiplier strongly depends on dimensionless gas velocity, it is relatively independent of superficial liquid velocity and channel size.

Jung and Radermacher [105] ran a considerable number of experiments with both pure and mixed refrigerants flowing within stainless steel tubes with a diameter of 9.1 mm and developed a simple correlation for predicting the two-phase flow pressure drop based on Martinelli's parameter. In their correlation, the two-phase frictional multiplier depends on quality and reduced pressure, as given in Table 4.

Ide and Matsumura [33] studied the effects of channel geometry on the two-phase flow pressure drop in rectangular channels. They used channels with different aspect ratios, hydraulic diameters, and inclination angles and found that the Lockhart–Martinelli method does not accurately predict the experimental results with low liquid superficial velocities and high inclination angles. They used the separated flow model and proposed a correlation that predicts the frictional pressure drop as a function of channel aspect ratio, inclination angle, Reynolds number, and void fraction. The pressure drop correlation that they proposed is given in Table 4.

Many efforts have been made to modify the Chisholm parameter to make the predicted pressure drop closer to the actual value measured experimentally. Mishima and Hibiki [106] studied two-phase flow of air and water in round capillary tubes with diameters ranging from 1 mm to 4 mm. They noticed that the Chisholm parameter should also be a function of channel diameter, rather than just the two-phase flow pattern. They studied the variation of the two-phase flow multiplier as a function of the Lockhart–Martinelli parameter for different diameters and observed that the Chisholm parameter decreases with the tube diameter. This led them to propose a modified Chisholm parameter that takes into account the diameter of the channel. For circular channels, the Chisholm parameter was proposed to be calculated by

$$C = 21(1 - e^{-0.333D}) \tag{15}$$

where D is the channel diameter in meters. For rectangular channels, the Chisholm parameter was recommended to be obtained by the following equation:

$$C = 21(1 - e^{-0.319D_h}) \tag{16}$$

where D_h is the hydraulic diameter.

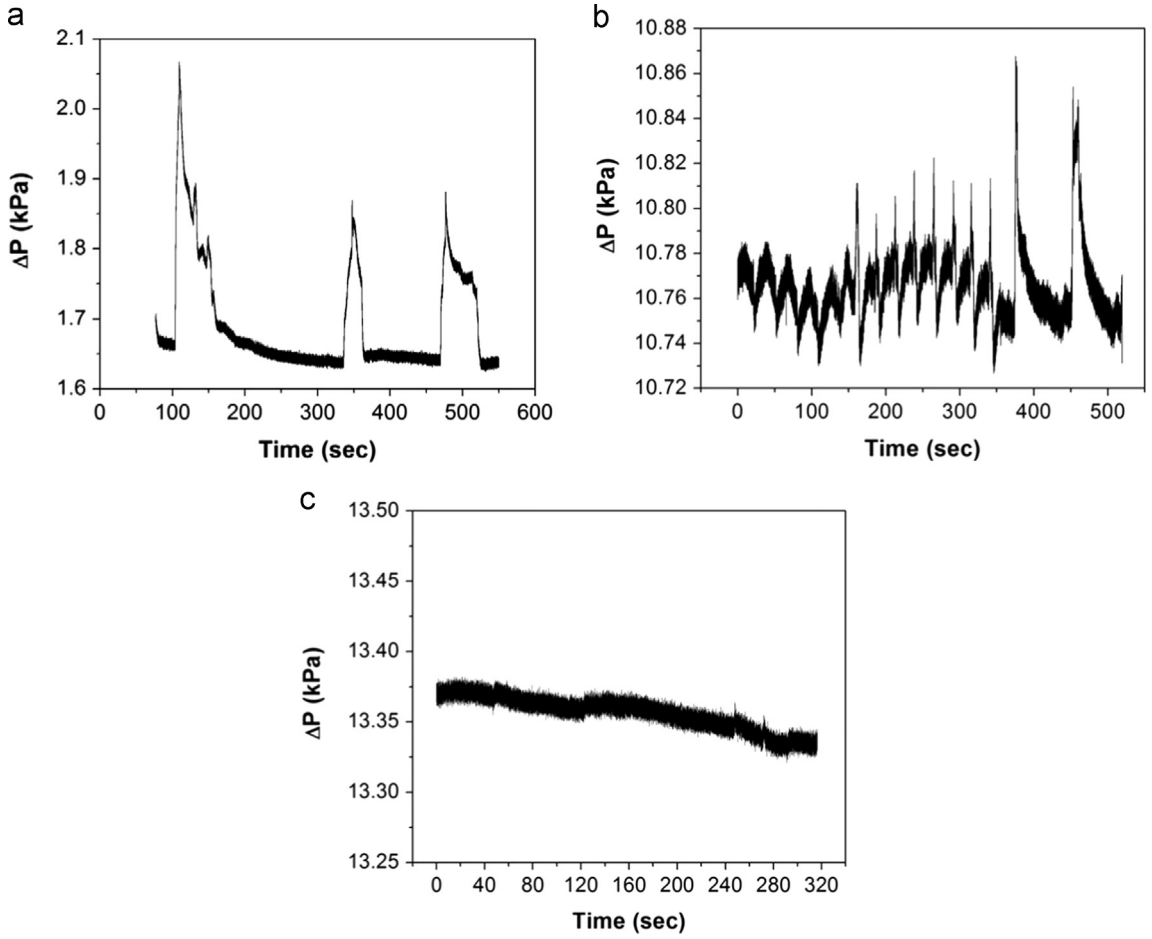

Fig. 4. The two-phase flow pressure drop signature reported by Grimm et al. [47]: (a) spikes in pressure drop signature due to slug formation for water flow rate of 0.1 mℓ min^{-1} and air flow rate of 330 sccm, (b) fluctuation in pressure drop due to film flow for water flow rate of 0.04 mℓ min^{-1} and air flow rate of 1981 sccm, (c) pressure drop signature for mist flow for water flow rate of 0.02 mℓ min^{-1} and air flow rate of 2311 sccm.

Table 4
Two-phase frictional pressure gradient correlation.

Author	Equation	Setup
Lockhart and Martinelli [64]	$\left(\frac{dP}{dz}\right)_{TP,F}=\left(\frac{dP}{dz}\right)_f\phi_f^2,\ \phi_f^2=1+\frac{C}{X}+\frac{1}{X^2}$	$D=1.49$–25.83 mm
	$X^2=\frac{\left(\frac{dP}{dz}\right)_f}{\left(\frac{dP}{dz}\right)_g}$, C_{vv}, C_{tv}, C_{vt}, and C_{tt} as given in Table 3	Water, oils, hydrocarbon
Friedel [101]	$\left(\frac{dP}{dz}\right)_{TP,F}=\left(\frac{dP}{dz}\right)_f\phi_f^2$	$D>4$ mm
	$\phi_f^2=(1-x)^2+x^2\left(\frac{v_g}{v_f}\right)\left(\frac{f_{go}}{f_{fo}}\right)+3.24x^{0.78}(1-x)^{0.224}\left(\frac{v_g}{v_f}\right)^{0.91}\left(\frac{\mu_g}{\mu_f}\right)^{0.19}\left(1-\frac{\mu_g}{\mu_f}\right)^{0.7}Fr_{TP}^{-0.045}We_{TP}^{-0.035}$	Air–water, air–oil, R12
	$Fr_{TP}=\frac{G^2}{gD_h\rho_h^2}$, $We_{TP}=\frac{G^2D_h}{\sigma\rho_{TP}}$, $\rho_{TP}=\frac{1}{xv_g+(1-x)v_f}$	
Müller-Steinhagen and Heck [102]	$\left(\frac{dP}{dz}\right)_{TP,F}=\left[\left(\frac{dP}{dz}\right)_f+2\left[\left(\frac{dP}{dz}\right)_g-\left(\frac{dP}{dz}\right)_f\right]x\right](1-x)^{1/3}+\left(\frac{dP}{dz}\right)_g x^3$	$D=4$–392 mm
		Air–water, hydrocarbons, refrigerants
Jung and Radermacher [105]	$\left(\frac{dP}{dz}\right)_{TP,F}=\left(\frac{dP}{dz}\right)_f\phi_f^2,\ \phi_f^2=12.82X_{tt}^{-1.47}(1-x)^{1.8}$	$D=9.1$ mm
	$X_{tt}=\left(\frac{\mu_f}{\mu_g}\right)^{0.1}\left(\frac{1-x}{x}\right)^{0.9}\left(\frac{\rho_g}{\rho_f}\right)^{0.5}$	Pure and mixed refrigerants
Ide and Matsumura [33]	$\phi_f=C(\theta)Re_{fo}^{-m}\chi_{tt}\left[\frac{(\beta+1)(\beta+\alpha)}{[\beta+2(1-\alpha)]^2}\right]^{-0.625}\left[\frac{\alpha}{(1-\alpha)^2}\right]^{1.5}$	$D=7.3$–21.4 mm
	χ_{tt} is the Lockhart–Martinelli parameter for turbulent liquid and gas flow turbulent	Air–water
	$m=0.3, C(\theta)=0.57+2.07\times10^{-2}\theta-1.818\times10^{-4}\theta^2$	$D_h>10$ mm
	$m=1.0, C(\theta)=170+11.18\theta-9.63\times10^{-2}\theta^2$	$D_h<10$ mm
Wambsganss et al. [107]	$\left(\frac{dP}{dz}\right)_{TP,F}=\left(\frac{dP}{dz}\right)_f\phi_f^2,\phi_f^2=1+\frac{C}{X}+\frac{1}{X^2}$	$D_h=5.44$ mm
	$C=f(X,Re_{fo})=aX^b$, $a=-2.44+0.00939Re_{fo}$, $b=-0.938+0.000432Re_{fo}$	Air–water
Wang et al. [99]	For $G\geq200$ kg/m^2 s, $\left(\frac{dP}{dz}\right)_{TP,F}=\left(\frac{dP}{dz}\right)_g\phi_g^2,\ \phi_g^2=1+9.4X^{0.62}+0.564X^{2.45}$	$D=6.5$ mm
	For $G<200$ kg/m^2 s, $\left(\frac{dP}{dz}\right)_f=\left(\frac{dP}{dz}\right)_f\phi_f^2,\ \phi_f^2=1+\frac{C}{X}+\frac{1}{X^2}$	R22, R134a, R407C
	$C=4.566\times10^{-6}X^{0.128}Re_{fo}^{0.938}\left(\frac{v_f}{v_g}\right)^{2.15}\left(\frac{\mu_f}{\mu_g}\right)^{5.1}$	
Zhang and Webb [70]	$\phi_f^2=(1-x)^2+2.87x^2\left(\frac{P}{P_c}\right)^{-1}+1.68x^{0.8}(1-x)^{0.25}\left(\frac{P}{P_c}\right)^{-1.64}$	$D_h=2.13$ mm
		R-134a, R22, R404a
Mishima and Hibiki [106]	$\left(\frac{dP}{dz}\right)_{TP,F}=\left(\frac{dP}{dz}\right)_f\phi_f^2,\ \phi_f^2=1+\frac{C}{X}+\frac{1}{X^2}$	$D=1.05$–4.08 mm
	For rectangular channel, $C=21[1-\exp(-319D_h)]$	
	For circular tube, $C=21[1-\exp(-333D)]$	
Yang and Webb [108]	$\left(\frac{dP}{dz}\right)_{TP,F}=-0.87Re_{eq}^{0.12}f_{fo}\frac{G_{eq}^2v_f}{D_h}$, $Re_{eq}=\frac{G_{eq}D_h}{\mu_f}$, $G_{eq}=G\left[(1-x)+x\left(\frac{\rho_f}{\rho_g}\right)^{0.5}\right]$	$D_h=1.56$–2.64 mm
		R12
Tran et al. [80]	$\left(\frac{dP}{dz}\right)_{TP,F}=\left(\frac{dP}{dz}\right)_f\phi_f^2,\ N_{conf}=\sqrt{\frac{\sigma}{g(\rho_f-\rho_g)D^2}}$	$D=2.4$–2.92 mm
	$\phi_f^2=1+\left[4.3\frac{(dP/dz)_{go}}{(dP/dz)_{fo}}-1\right]\left[N_{conf}x^{0.875}(1-x)^{0.875}+x^{1.75}\right]$	Refrigerants
Chen et al. [69]	$\left(\frac{dP}{dz}\right)_{TP,F}=\left(\frac{dP}{dz}\right)_{f,Friedel}\Omega,\ Bo^\star=g(\rho_f-\rho_g)\frac{(D_h/2)^2}{\sigma}$	$D=1.02$–9 mm
	for $Bo^\star<2.5, \Omega=\frac{0.0333Re_{fo}^{0.45}}{Re_g^{0.09}(1+0.4\exp(-Bo^\star))}$	Air–water, R410A, ammonia
	For $Bo^\star\geq2.5$, $\Omega=\frac{We_{TP}^{0.2}}{(2.5+0.06Bo^\star)}$	
Lee and Lee [109]	$\left(\frac{dP}{dz}\right)_{TP,F}=\left(\frac{dP}{dz}\right)_f\phi_f^2,\ \phi_f^2=1+\frac{C}{X}+\frac{1}{X^2},\ \psi=\frac{\mu_f j_f}{\sigma},\ \lambda=\frac{\mu_f^2}{\rho_f\sigma D_h}$	$D_h=0.78$–6.67 mm
	$C=A\lambda^q\psi^rRe_{fo}^s$	Air–water
	For laminar liquid-laminar gas flow $A=6.833\times10^{-8}$, $q=-1.317$, $r=0.719$, $s=0.557$	
	For laminar liquid-turbulent gas flow $A=6.185\times10^{-2}$, $q=0$, $r=0$, $s=0.726$	
Saisorn and Wongwises [29]	$\left(\frac{dP}{dz}\right)_{TP,F}=\left(\frac{dP}{dz}\right)_f\phi_f^2,\ \phi_f^2=1+\frac{C}{X}+\frac{1}{X^2},\ \psi=\frac{\mu_f j_f}{\sigma},\ \lambda=\frac{\mu_f^2}{\rho_f\sigma D_h}$	$D=0.15$–0.53 mm
	$C=7.599\times10^{-3}\lambda^{-0.631}\psi^{0.005}Re_{fo}^{-0.008}$	Air–water
Yu et al. [71]	$\left(\frac{dP}{dz}\right)_{TP,F}=\left(\frac{dP}{dz}\right)_f\phi_f^2,\ \phi_f^2=\left[18.65\left(\frac{v_f}{v_g}\right)^{0.5}\left(\frac{1-x}{x}\right)\frac{Re_g^{0.1}}{Re_f^{0.5}}\right]^{-1.9}$	$D=2.98$ mm
		Water and ethylene glycol
Hwang and Kim [110]	$\left(\frac{dP}{dz}\right)_{TP,F}=\left(\frac{dP}{dz}\right)_f\phi_f^2,\ \phi_f^2=1+\frac{C}{X}+\frac{1}{X^2},\ C=0.227Re_{fo}^{0.452}X^{-0.32}N_{conf}^{-0.82}$	$D=0.244$–0.792 mm
		R134a

Table 4 (*continued*)

Author	Equation	Setup
Sun and Mishima [103]	For $Re_f < 2000$ and $Re_g < 2000$ $\left(\frac{dP}{dz}\right)_{TP,F} = \left(\frac{dP}{dz}\right)_f \phi_f^2 = 1+\frac{C}{X}+\frac{1}{X^2}$ $C = 26\left(1+\frac{Re_f}{1000}\right)\left[1-\exp\left(\frac{-0.153}{0.27N_{conf}+0.8}\right)\right]$ For $Re_f \geq 2000$ or $Re_g \geq 2000$ $\left(\frac{dP}{dz}\right)_{TP,F} = \left(\frac{dP}{dz}\right)_f \phi_f^2 = 1+\frac{C}{X}+\frac{1}{X^2}$, $C = 1.79\left(\frac{Re_g}{Re_f}\right)^{0.4}\left(\frac{1-x}{x}\right)^{0.5}$	$D_h = 0.506$–12 mm Air–water, refrigerants
Li and Wu [111]	$\left(\frac{dP}{dz}\right)_{TP,F} = \left(\frac{dP}{dz}\right)_f \phi_f^2 = 1+\frac{C}{X}+\frac{1}{X^2}$, $Bo = \frac{g(\rho_f-\rho_g)D_h^2}{\sigma}$ For $Bo \leq 1.5$, $C = 11.9Bo^{0.45}$ For $1.5 < Bo \leq 11$, $C = 109.4(BoRe_f^{0.5})^{-0.56}$	$D_h = 0.148$–3.25 mm refrigerants, ammonia Refrigerants, ammonia
Zhang et al. [112]	$\left(\frac{dP}{dz}\right)_{TP,F} = \left(\frac{dP}{dz}\right)_f \phi_f^2$, $\phi_f^2 = 1+\frac{C}{X}+\frac{1}{X^2}$, $C = 21[1-\exp(-0.142/N_{conf})]$	$D_h = 0.07$–6.25 mm Air–water, refrigerants, ammonia
Li and Wu [113]	For $Bo < 0.1$ $\left(\frac{dP}{dz}\right)_{TP,F} = \left(\frac{dP}{dz}\right)_f \phi_f^2$, $\phi_f^2 = 1+\frac{C}{X}+\frac{1}{X^2}$, $C = 5.60Bo^{0.28}$ For $Bo \geq 0.1$ and $BoRe_f^{0.5} \leq 200$ $\left(\frac{dP}{dz}\right)_{TP,F} = \left(\frac{dP}{dz}\right)_f \phi_{fo}^2$, $\phi_f^2 = (1-x)^2+2.87x^2\frac{P_c}{P}+1.54Bo^{0.19}\left(\frac{\rho_f-\rho_g}{\rho_{TP}}\right)^{0.81}$	$D_h = 0.148$–3.25 mm Refrigerants, ammonia
Lee and Mudawar [95]	$\phi_f^2 = 1+\frac{C}{X}+\frac{1}{X^2}$ For laminar liquid-laminar gas flow, $C = 2.16Re_{fo}^{0.047}We_{fo}^{0.60}$ For laminar liquid-turbulent gas flow, $C = 1.45Re_{fo}^{0.25}We_{fo}^{0.23}$	$D_h = 348$ μm R134a

So far, the two-phase flow pressure drop is reviewed for general applications. The applications of the two-phase flow span a wide range of working conditions. An accurate knowledge of the two-phase flow pressure drop can be obtained by identifying the working condition of each particular application separately. In Section 4, the two-phase flow pressure drop is studied for PEM fuel cell applications. The section reviews the effect of different working conditions of a PEM fuel cell on the two-phase flow pressure drop within the channels.

4. Pressure drop with PEM fuel cell application

In this section, the two-phase flow pressure drop in PEM fuel cell flow channels is reviewed. The two-phase flow in PEM fuel cells has some unique characteristics, such as small length scales, a special liquid water introduction mechanism into the gas channel, and different surface energies of the channel walls. The small length scale of PEM fuel cell gas channels diminishes the effects of gravity on the two-phase flow and makes the surface tension effects more dominant. This is different from macro-scale channels where gravity has a dominant effect on the two-phase flow. Furthermore, in PEM fuel cells, liquid water is continuously produced in the catalyst layer and is introduced into the gas channel through the porous GDL. The water emergence from the surface of the GDL within the gas channel occurs at preferential locations. This water introduction mechanism is different from what happens in conventional channels where the two phases are usually introduced and mixed at the inlet of the channel. Moreover, the two-phase flow in PEM fuel cells occurs in channels with GDL as one of the walls and graphite or metal as the other three walls. This yields different surface characteristics of the walls that bind the two-phase flow in PEM fuel cells. Also the channel corners may affect the water transport mechanism if the Concus–Finn condition is met [114]. Finally, the non-uniform GDL intrusion into the gas channels may affect the two-phase flow pressure drop in PEM fuel cell gas channels. Because the cell compression is not uniform in the plane of the flow field, the GDL intrusion into the gas channel will not be also uniform. The GDL intrusion near the edges of the flow field is greater than the GDL intrusion in the central region of the cell. This leads to a higher pressure drop in the side channels compared to the interior channels and therefore results in a nonuniform pressure drop over the flow channels.

In this section, the effect of different PEM fuel cell working conditions on the two-phase flow pressure drop in fuel cell gas channels is reviewed. Pressure drop hysteresis, defined as the pressure drop while the gas flow rate is increased and then decreased, is also discussed. The section ends with reviewing the models that have been proposed for predicting the two-phase flow pressure drop in PEM fuel cell gas channels. Table 5 lists the literature that has studied the two-phase flow pressure drop in PEM fuel cell gas channels.

4.1. Two-phase flow pressure drop for different flow patterns in PEM fuel cell

Different from single-phase flow in which each flow rate results in a specific pressure drop, a particular two-phase pressure drop can be obtained from different combinations of liquid and gas flow rates. The two-phase pressure drop can be correlated to the flow pattern within the gas channel. Grimm et al. [47] studied the two-phase flow pressure drop in a simulated PEM fuel cell gas channel by providing air and water at different flow rates corresponding to slug flow, film flow and mist flow. Fig. 4 shows the pressure drop they measured at different flow patterns. The two-phase flow pressure drop of slug flow contains large spikes that repeat with long time intervals. Each spike of the pressure drop profile represents the formation of a slug in the gas channel. As the slug forms, the channel cross section decreases and the pressure drop increases until the pressure can provide enough force to remove the slug from the channel. Increasing the air flow rate to film flow and ultimately mist flow makes the pressure drop spikes shorter. The minimal oscillation of the pressure drop profile can be

observed in mist flow. This is due to the large gas to liquid ratio that makes the mist flow behave similarly to single-phase flow. Similar pressure drop profiles for these two-phase flow patterns have been reported in other studies [44,46].

4.2. Two-phase flow pressure drop and cell performance

The pressure drop can be considered as a diagnostic tool that describes the amount of accumulated liquid water within the gas channel. Liquid water can accumulate inside the gas channel when the water production rate is greater than the water removal rate. The accumulated liquid water blocks the transport of the reactants and consequently lowers the performance of the cell. The accumulated water in the gas channel also causes a pressure drop by resisting the gas flow. Liu et al. [128] used a transparent cell and studied the water flooding in gas channels by simultaneously monitoring the cell performance and the cathode and anode pressure drop, as shown in Fig. 5. It can be observed from the figure that the cell performance degradation is accompanied by an increase in the cathode pressure drop. This observation has been

Table 5
Literatures studying the pressure drop in PEM fuel cells.

Author	Area of focus	Experiment type	Major conclusion
English [63]	Two-phase flow pressure drop	Ex situ	A pressure drop correlation based on LM method is proposed
Zhang [43]	Two-phase flow pressure drop	Ex situ	A negative slope in pressure drop vs. superficial gas velocity indicates a flow pattern change from a non-uniform to an uniform pattern
Zhang [52]	Two-phase flow pressure drop	Ex situ	Pressure drop increases with the inclination angle
Lu [44]	Two-phase flow pressure drop	Ex situ	A large fluctuation in the pressure drop is noted for the slug flow, moderate oscillation for film flow and minimal fluctuation for mist flow
Yu [115]	Two-phase flow pressure drop	Ex situ	The pressure drop results indicate that the annular purge is more appropriate for removing liquid water in anode
Chen [53]	Two-phase flow pressure drop	Ex situ	The porous insert causes a four-fold pressure drop compared to hollow channels
Lu [45]	Two-phase flow pressure drop	Ex situ	Sinusoidal channel results in lower pressure drop than rectangular and trapezoidal. Hydrophilic channel surface has lower two phase flow multiplier at lower superficial gas velocity
Zhang [46]	Two-phase flow pressure drop	Ex situ	A pressure drop correlation based on LM method is proposed
Radhakrishnan [116]	Two-phase flow pressure drop	Ex situ	While GDL compression does not change the pressure drop significantly in parallel flow field, it causes a significant pressure drop increase in serpentine flow field
Allen [117]	Two-phase flow pressure drop	Ex situ	Pressure drop is used to describe flow patterns
Hsieh [118]	Two-phase flow pressure drop	In situ	The interdigitated flow channel yields the highest pressure drop compared to serpentine, parallel and mesh configuration
Grimm [47]	Two-phase flow pressure drop	Ex situ	Different pressure drop correlations are proposed for slug, film and mist flow
Anderson [119]	Two-phase flow pressure drop hysteresis	Ex situ	Two phase flow pressure drop hysteresis disappears at stoichiometries of 5 and higher. Initial water balance affects the hysteresis pattern
Anderson [120]	Two-phase flow pressure drop hysteresis	Ex situ	The pressure drop hysteresis becomes less significant at higher temperatures
Anderson [121]	Two-phase flow pressure drop hysteresis	In situ	The modified LM approach given in [46] can predict the two-phase flow pressure drop in an ascending approach
Rodatz [122]	Fuel cell stack operation	In situ	The pressure drop is observed to decrease with the cell's current density
Barbir [123]	Flooding	In situ	Flooding or drying can be diagnosed by monitoring the pressure drop and resistance simultaneously
Yamada [124]	Flooding	In situ	The pressure drop measured during flow field switch from parallel to interdigitated indicates the level of GDL flooding
Jiao [125]	Cold start of PEM fuel cell	In situ	The ice blockage in flow channel and GDL leads to a significant pressure drop through cathode flow field.
Reference	Area of focus	Experiment type	Major conclusion
Trabold [51]	Liquid water accumulation	In situ	Pressure drop has been employed as a diagnostic tool to study the water accumulation. While the pressure drop was observed to significantly increase in the cathode, it has been observed that it slightly changes in the anode
Ma [126]	Liquid water accumulation	In situ	The pressure drop results can be used to determine the proper gas velocity required to remove liquid water
Ge [127]	Liquid water accumulation	In situ	Anode pressure drop is used to evaluate water transport between anode and cathode during the operation of the cell
Liu [128]	Liquid water accumulation	In situ	The existence of water is found to be the main reason of pressure drop in the flow channels
Ito [129]	Liquid water accumulation	In situ	The differential pressure drop between the inlet and outlet of an interdigitated cell can be used to estimate the level of water saturation within the GDL
Hussaini [10]	Liquid water accumulation	In situ	Two phase flow pressure drop is utilized as a diagnostic tool that describes the amount of liquid water in gas channel
Spernjak [130]	Liquid water accumulation	In situ	Monitoring the pressure drop, current density, and water volume simultaneously can be used to identify three stages of water evolution
Kandlikar [54]	Flow maldistribution	In situ/ex situ	

Table 5 (*continued*)

Author	Area of focus	Experiment type	Major conclusion
			A new technique is proposed to calculate instantaneous flow in each channel based on the measured pressure drop
Kandlikar [131]	GDL intrusion	Ex situ	The GDL intrusion should be considered for an accurate estimation of total pressure drop
Akhtar [132]	Liquid water transport	Ex situ	The pressure drop is used to define the optimum channel geometry in terms of liquid water removal
Chen [133]	Liquid water transport	Ex situ	The dominant frequency of the pressure drop may be used as a diagnostic tool for water removal
Dillet [134]	Liquid water transport	In situ	Clogging and unclogging can be detected by monitoring the pressure drop and cell voltage simultaneously
Blanco [135]	Liquid water transport	In situ	Pressure drop is used to evaluate water transport between anode and cathode
Colosqui [136]	Liquid water transport	Ex situ	Monitoring the pressure drop over time is used to describe drop and slug formation
Liu [137]	Flow channel design	In situ	Pressure drop is used to design flow channels with effective water removal
Taccani [138]	Flow filed geometry	In situ	The serpentine flow field results in higher pressure drop than the parallel flow field
Bachman [139]	Channel length	In situ	Although longer gas channel exhibit larger pressure drop, it shows a more stable cell performance compared to shorter channels

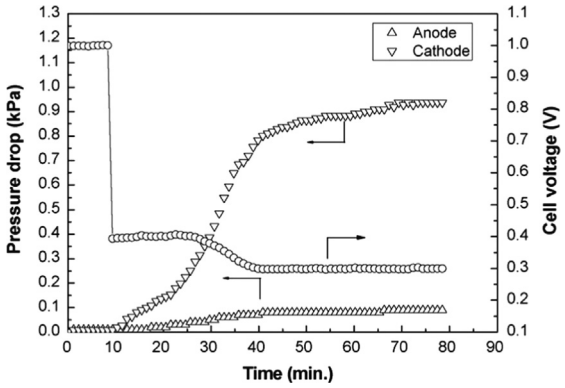

Fig. 5. Cell performance and the cathode and anode pressure drop reported by Liu et al. [128]. Parallel gas flow field fuel cell operating at 25 °C and 69.6 $m\ell\ min^{-1}$ oxygen flow rate and 139.3 $m\ell\ min^{-1}$ hydrogen flow rate.

reported to be an indication of the liquid water accumulating within the gas channels. Another remarkable observation of this study is the higher pressure drop of the cathode compared to the anode. The amount of water produced in the cathode is much greater than the water accumulated in the anode, either by water condensation in the humidified anode gas or back diffusion of water from the cathode to the anode.

Dillet et al. [134] performed an in situ test and measured the pressure drop and cell voltage in a single channel segmented fuel cell. They were able to define the channel clogging and unclogging sequences by analyzing the simultaneous records of the pressure drop and the cell voltage.

4.3. Effect of flow field geometry on the two-phase flow pressure drop

Flow field geometry has been known to have a significant impact on the mass transport of the reactants and products, as well as the pressure drop between the inlet and the outlet of the flow channels [140]. An appropriate flow channel design has been mentioned to be the most successful strategy in addressing water flooding issues [9]. Flow field geometry also impacts the current distribution and the cell performance [141]. A comprehensive review of the flow field design has been done by Li and Sabir [141]. The common flow field designs for PEM fuel cells include parallel channels, serpentine flow field, and interdigitated flow field [142–144]. In a parallel flow field, straight parallel channels connect the inlet and outlet headers. Parallel flow fields may suffer from unequal liquid water distributions within the channels. In this situation, the low pressure drop cannot remove water slug from the gas channels [142,143]. This can lead to flow maldistribution that will ultimately cause reactant starvation in some channels and excess reactants in other channels. The serpentine flow field is made of one or more long channels that pass through the whole bipolar plate via several bends. These bends cause a relatively high pressure drop that can facilitate water removal from the channels. Despite parallel and serpentine flow channels that connect the inlet header to the outlet header, an interdigitated flow field design includes channels that are connected into either inlet or outlet headers. In this type of flow field, reactants penetrate into the porous GDL and permeate through to reach the outlet channels. This induces a large pressure drop which facilitates water removal from the porous GDL. Although the improved water removal in an interdigitated flow field makes it an ideal type of flow field for high current densities, its high pressure drop characteristic results in an increased parasitic power within the system.

Spernjak et al. [130] studied the effect of the flow field design on the cell performance and the two-phase flow pressure drop in anode and cathode. While the serpentine flow field was reported to result in a higher limiting current density compared to a parallel and interdigitated flow field, it has been argued that serpentine flow field configuration exhibits a substantially higher pressure drop compared to parallel and interdigitated flow fields. Similar results have been reported by Taccani and Zuliani [138] as they studied the effect of the flow field geometry on the overall performance of polybenzimidazole PEM fuel cells working at a higher temperature range (120–180 °C).

Hsieh et al. [140] measured the pressure drop of PEM fuel cells with four different flow fields. The pressure drops have been measured in interdigitated, serpentine, parallel, and mesh flow fields with an active area of 22.5 mm × 22.5 mm when each cell was operating with 60 sccm air flow rate. Fig. 6 shows the pressure drop they measured during 180 min operation of the cell. The figure shows that the maximum pressure drop occurs in the cell with an interdigitated flow field and the minimum pressure drop occurs in the mesh flow channel. The figure also shows that the

pressure drop of the serpentine flow field is higher than the pressure drop of the parallel flow field.

Other than the flow field design, channel geometry also impacts the performance of the cell as well as the liquid water transport mechanism. Owejan et al. [16] used neutron radiography to acquire liquid water distribution in operating fuel cells with different cross-sectional geometries. They used triangular and rectangular channels with the same cross-sectional areas and noticed that triangular channels retain less water compared to rectangular channels. The effects of the gas channel length, width, depth, and rib size on the two-phase flow pressure drop have also been the subject of several studies [45,132,139].

Akhtar et al. [132] studied the minimum pressure drop required to remove a condensate from gas channels with different cross-sectional geometries, as shown in Fig. 7. They found that the minimum pressure drop that can transport the droplet depends on the normalized droplet volume. The normalized droplet volume was defined as the channel filling droplet of 1 mm in length. For small droplets with normalized volume less than 1, the pressure drop was observed to decrease as the normalized water droplet volume increased, as shown in Fig. 8. The figure suggests that a small amount of liquid water (normalized volume of less than 1) can be efficiently removed in a wide channel (R1 and R3). For larger drops with a normalized droplet volume of greater than 1 (not shown), it was reported that the pressure drop remains nearly constant for different normalized volumes and for each cross section. However, the minimum pressure drop required to remove drops was reported to be maximum for cross section R4 and minimal for cross section R1.

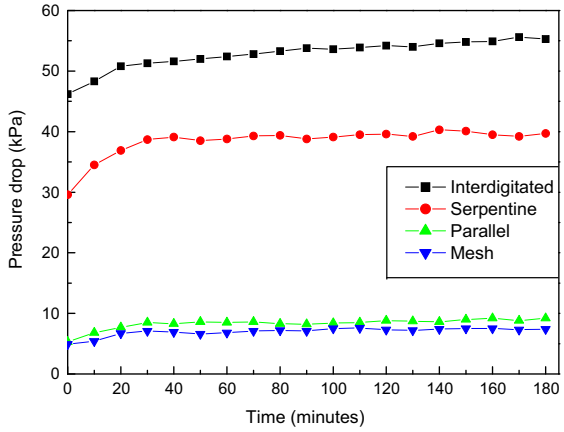

Fig. 6. Pressure drop measured in different flow fields reported by Hsieh et al. [140].

Lu et al. [45] studied the effect of channel cross-sectional geometry on the two-phase flow properties in parallel gas channels. They tested three different cross-sectional geometries, rectangular, sinusoidal, and trapezoidal and observed that the sinusoidal channel causes the lowest two-phase flow frictional multiplier, ϕ_g^2. They also compared flow images for different channel geometries and noticed that the flow pattern in the sinusoidal channel is characterized by multiple small slugs rather than fewer long slugs as can be observed in rectangular and trapezoidal channels. Moreover, a more uniform water distribution was reported within sinusoidal channels compared to rectangular and trapezoidal channels.

The other geometrical parameter that also impacts the pressure drop is the channel length. Bachman et al. [139] measured the cell output and the pressure drop of parallel flow channels with different lengths of 5 cm, 15 cm, and 25 cm. It has been reported that although longer channels suffer from a higher pressure drop, they can improve the performance of the cell. The cell with a 5 cm gas channel exhibited an erratic and unstable performance, while the cell with a 25 cm gas channel had a stable output. The unsteady and high accumulation of water within the 5 cm channel has been mentioned to be the main reason of its low and unstable performance.

Channel corner angle can also impact water transport within the gas channel. According to Concus–Finn criteria, if the droplet static contact angle, θ, be smaller than $\pi/2-\alpha$, where α is the half-angle of the channel cross-sectional corner, liquid water can wick into the channel corner and transport along the corner within the gas channel. Rath and Kandlikar [145] utilized the Concus–Finn condition to determine the corner angle at which a water droplet can fill the corner. The corner is made of 2 surfaces, the GDL and

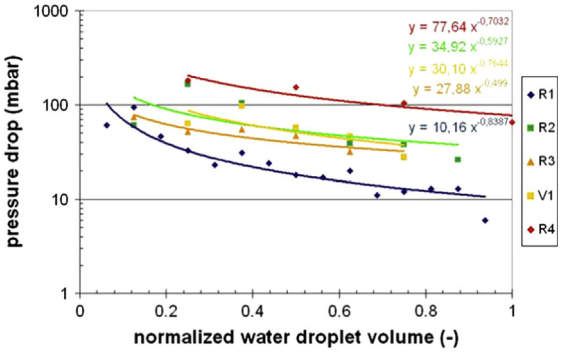

Fig. 8. Minimum pressure drop required for drop removal reported by Akhtar et al. [132].

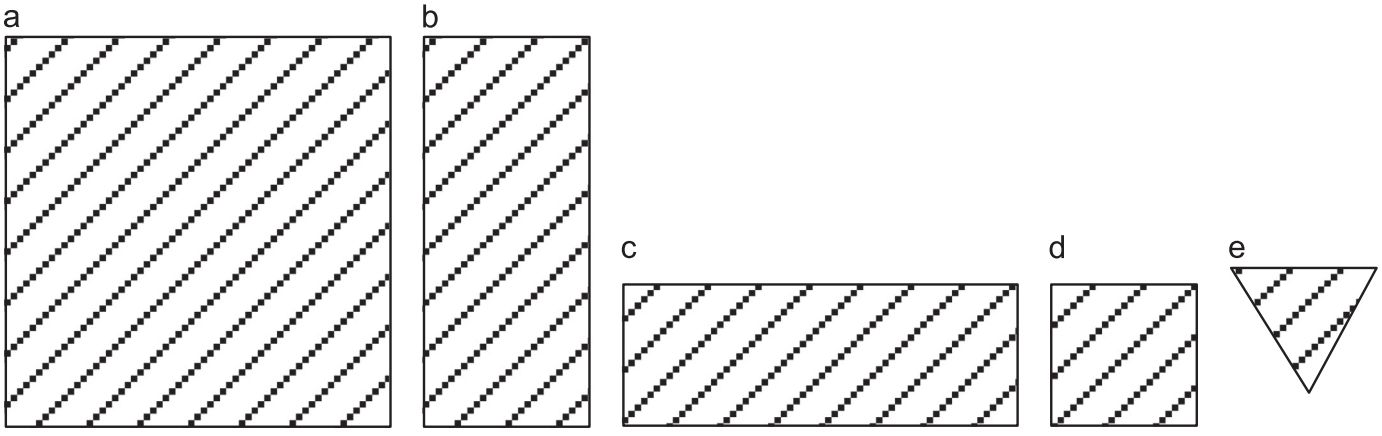

Fig. 7. Cross-sectional geometries of the gas channels that were considered by Akhtar et al. [132] (a) R1, 1 mm × 1 mm, (b) R2, 0.5 mm × 1 mm, (c) R3, 1 mm × 0.5 mm, (d) R5, 0.5 mm × 0.5 mm, and (e) V1, 0.5 mm and 53°.

the surface channel, each with different surface energies. It has been reported that the GDL corners do not fill when the corner angle is less than 52°.

4.4. Effect of gas stoichiometry on the two-phase flow pressure drop

The stoichiometry ratio describes the ratio of the supplied reactant flow to the reactant consumption rate. The concentration loss caused by water flooding can be avoided, in part, by increasing the stoichiometric ratio. Flow stoichiometry can also convectively remove water from the gas channel [121]. While a high stoichiometry may be helpful in increasing the mass transport rate of reactants and avoiding the flooding, an excess stoichiometry, on the other hand, can cause some major disadvantages. Some common problems caused by high stoichiometries are membrane dehydration and decreased reactant utilization [146,147]. Ous and Arcoumanis [148] studied the effect of different air and hydrogen stoichiometries on the accumulation of water in the cathode and anode of a transparent PEM fuel cell. It has been reported that an increased air stoichiometry is capable of removing all of the liquid water from the cathode channels without causing membrane dehydration. However, elevated hydrogen stoichiometries were mentioned to be incapable of removing liquid water from inside the cell.

Lu et al. [44] studied the two-phase flow in PEM fuel cell parallel flow channels for different air stoichiometries and noticed that air stoichiometries of less than 5 typically yield slug flow with large pressure drop fluctuation. Higher stoichiometries were reported to cause film flow with water film forming on hydrophilic channels. The pressure profile of film flow was characterized by smaller but more frequent fluctuations compared to slug flow. Further increase in the stoichiometry ratio was reported to result in mist flow with less water being accumulated within the flow channels and therefore minimal pressure oscillation.

Anderson et al. [119] studied the effect of the flow stoichiometry on the two-phase flow pressure drop in a non-operating PEM fuel cell. Fig. 9 shows the pressure drop they measured for different stoichiometries and for ascending and descending approaches. Ascending describes an increasing gas flow rate and descending describes a decreasing gas flow rate. Further discussion of the differences between ascending and descending results is given in Section 4.8 where pressure drop hysteresis is reviewed. Fig. 9 shows that increasing the stoichiometry ratio increases the pressure drop for each simulated current density. This originates from the pressure drop being proportional to the gas flow rate. A similar trend in pressure drop has been reported by Lin and Nguyen [147] as they studied water flooding in PEM fuel cells for different GDLs and at different stoichiometries.

Hussaini and Wang [10] calculated the two-phase flow frictional multiplier, ϕ, for different flow stoichiometries and noticed that increasing the flow stoichiometry decreases the two-phase flow frictional multiplier. This can be interpreted as more water being removed from inside the gas channel as the stoichiometry increases.

4.5. Effect of wettability on the two-phase flow pressure drop

Liquid water behavior on a solid surface is characterized by the surface wettability. While water spreads on hydrophilic surfaces, which are defined as the surfaces with contact angles less than 90°, it beads up on hydrophobic surfaces that make contact angles of greater than 90°. Surface wettability also affects the water transport mechanism. For a hydrophilic channel with the Concus–Finn condition being satisfied [114], liquid water wicks into the corner and drains via capillary flow. However, for a hydrophobic channel, water pins on the surface and forms slugs. A similar behavior of water droplets can be observed on the GDL surface. A

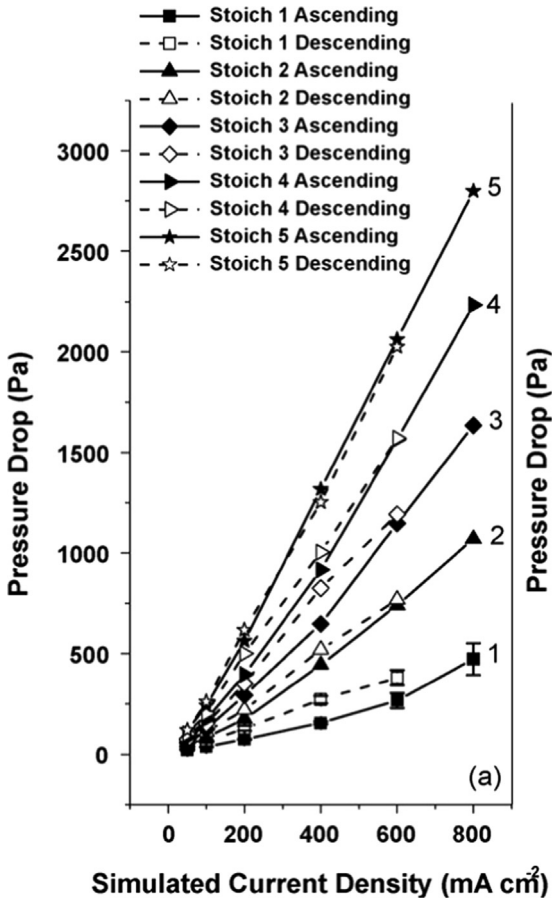

Fig. 9. Effect of the gas stoichiometry on the pressure drop reported by Anderson et al. [119].

water droplet can be detached from the GDL surface only if the shear gas flow can provide the required drag force to exceed the surface adhesion force [7]. The drag force applied on the droplet from the core gas flow depends on the projected area of the droplet and consequently depends on the droplet contact angle on the surface of the GDL.

Lu et al. [45] studied the effect of channel surface wettability on the two-phase flow in parallel gas channels. Fig. 10 shows the two phase flow frictional multiplier, ϕ_g^2, at different superficial liquid and gas velocities. The figure shows a lower ϕ_g^2 for a hydrophilic channel with lower water flow rate (left plot) and a higher ϕ_g^2 for a hydrophilic channel with higher water flow rate (right plot). The former was explained by the more uniform distribution of water within the gas channel, and the latter was explained by water film flow as the consequence of the Concus–Finn condition being met. Finally they concluded that although hydrophilic channels can cause certain water accumulation within the flow channels, they are still the superior channel surface treatment in terms of flow distribution compared to uncoated and hydrophobic channels.

GDL wettability has been reported to impact water condensation at low current densities. Ge and Wang [127] studied liquid water formation and transport in PEM fuel cells with hydrophobic and untreated GDL by comparing the pressure drop and the performance of the cell running at 0.2 A cm^{-2}. It has been reported that for a hydrophobic GDL, water is more prone to condense on the surface of the channel rather than inside the hydrophobic pores of the GDL. The accumulation of the condensed water on the surface of the hydrophobic GDL causes channel flooding with the anode pressure drop being increased. Channel flooding has reported to be eliminated by replacing the hydrophobic GDL with an untreated one. In contrast to

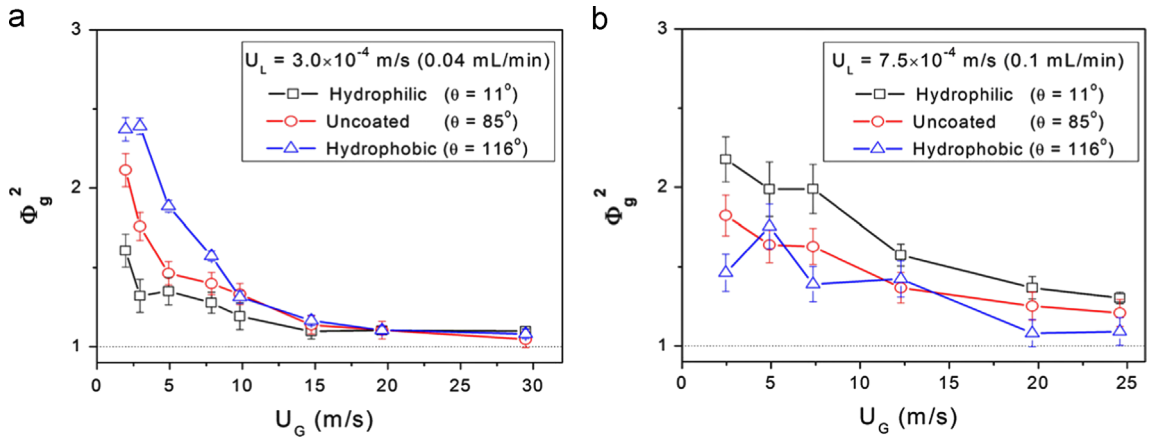

Fig. 10. Effect of channel wall surface energy on the two-phase flow frictional multiplier reported by Lu et al. [45]. (a) $j_f = 3.0 \times 10^{-4}$ m/s, (b) $j_f = 7.5 \times 10^{-4}$ m/s. The horizontal axis, U_G, is the superficial gas velocity.

the anode pressure drop for hydrophobic GDL, where the pressure continuously increased, the anode pressure drop for untreated GDL was reported to remain almost constant. This suggests a sharp difference between the water distribution at a low current density in the anode with hydrophobic GDL versus the anode with untreated GDL.

While Lu et al. [45] and Ge and Wang [127] reported that the surface characteristics of the GDL and channel walls can impact the pressure drop, Grimm et al. [47] has discussed that the channel surface characteristic does not affect the two-phase flow pressure drop in PEM fuel cell flow channels. They studied the two-phase flow in the gas channels of a PEM fuel cell in an ex situ setup that included GDL as one of the sidewalls. They used three channel treatments of hydrophobic, hydrophilic, and untreated, with contact angles of 116°, 11°, and 86°, respectively, and recorded the pressure drop along the flow channels. The effect of channel surface energy on the pressure drop was mentioned to be negligible in their studies.

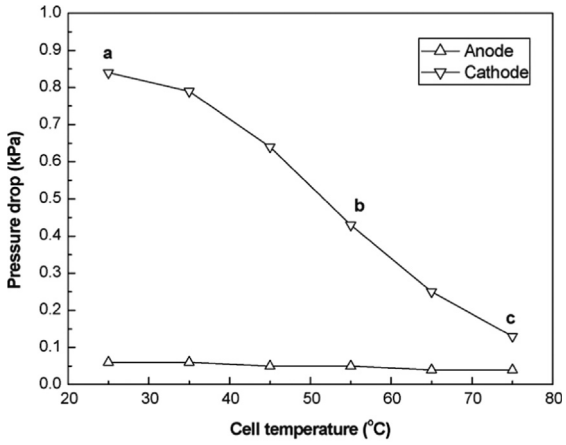

Fig. 11. Effect of temperature on two-phase flow pressure drop reported by Liu et al. [128].

4.6. *Effect of temperature on the two-phase flow pressure drop*

One of the most important parameters that can significantly affect the water content within the PEM fuel cell flow channels is the temperature of the cell. The neutron imaging studies conducted by Hickner et al. [149], and Owejan et al. [150] and direct visualization experiments performed by Liu et al. [151] report that the water content in PEM fuel cell flow channels decreases as the temperature of the cell increases. An increased temperature has been reported to decrease the condensation of liquid water [151] and increase the convective water removal capacity of the gases supplied within the flow channels [121]. Although an elevated cell temperature enhances the kinetics of the electrochemical reaction, which results in more water being produced during the operation of the cell, the enhanced water removal capacity of the reactant has a more dominant impact on water balance within the cell [151].

Ous and Arcoumanis [148] studied the accumulation of liquid water in serpentine flow channels of a transparent PEM fuel cell working at different temperatures between 30 °C and 60 °C. They noticed that a cell temperature of 60 °C is capable of evaporating all of the liquid water in the channels and enhancing the performance of the cell. The images taken from flow channels showed that the amount of liquid water decreased as the temperature was increased. A temperature of 60 °C was mentioned to result in minimal water content within the cell and an improved performance of the cell. However, an elevated cell temperature may not always be desirable as it may cause membrane dehydration during the operation of the cell [152,153].

Liu et al. [128] studied the effect of temperature on the liquid water accumulation and two-phase flow pressure drop in an operating cell. They ran a transparent PEM fuel cell at temperatures between 25 °C and 75 °C and observed that the amount of liquid water within parallel flow channels decreases by increasing the temperature. The two-phase flow pressure drop measurements in their study, as shown in Fig. 11, revealed that while the two-phase flow pressure drop in the cathode decreases in elevated temperatures, the anode pressure drop shows no sign of variation. The latter has been justified by increased evaporation of the accumulated water while the former was explained based on the few amount of accumulated water within anode flow channels.

Yan et al. [154] measured the two-phase flow pressure drop in anode and cathode of a PEM fuel cell with a serpentine flow field that operated at different cell and humidification temperatures. It has been reported that for a constant cell temperature, increasing the cathode and/or anode humidification temperature increases the two-phase flow pressure drop in both electrode flow channels. Increasing the humidification temperature increases the water vapor in the reactants, and therefore, more water vapor will enter the cell flow channel to be condensed. Similar to the findings presented by Liu et al. [128], the variation of the cathode pressure drop was more dominant compared to the variation of the anode pressure drop.

Anderson et al. [121] studied the two-phase flow pressure drop in an operating PEM fuel cell at different temperatures by calculating the two-phase flow multiplier for ascending and descending gas supply. They reported that temperature has negligible impact on the two-

phase flow frictional multiplier in the ascending approach. However, the two-phase flow multiplier was mentioned to be decreasing as the temperature was increased in the descending approach. Such observations have been explained by the amount of liquid water that accumulates in the gas channel in ascending and descending approaches. Because water accumulation is not significant in the ascending approach, increasing the temperature impacts the water content within the flow channels and therefore the frictional multiplier does not change with the temperature. However, the considerable amount of liquid water accumulated in the descending approach can evaporate at higher temperatures and therefore the frictional multiplier decreases as the temperature increases.

The temperature of the cell and the reactant temperature determine the relative humidity of the anode and cathode flow channels. Convective water removal from flow channels depends on the relative humidity. A reactant flow with a low relative humidity has more capability to remove liquid water via evaporation. Cathode flooding can be partially mitigated at lower relative humidities with an improved cell performance [155–157].

The effect of relative humidity on the cathode pressure drop has been studied by Hussaini and Wang [10] with the results shown in Fig. 12. The general trend suggests that the frictional multiplier increases with the relative humidity. This is because of the reduced evaporation rate of the water produced at higher relative humidities. It can also be observed that the effect of the relative humidity on the pressure drop becomes more significant at lower current densities. For instance for 26% relative humidity, 0.2 A cm^{-2} current density, and flow stoichiometry of 4, the frictional multiplier is 1. However, the frictional multiplier increases up to 3.5 for the same flow stoichiometry but for 66% relative humidity. This large variation in the frictional multiplier is because of the low air flow rate at a low current density which is not capable of removing the condensates either by convective evaporation or inertia effects.

4.7. Effect of MPL on the two-phase flow pressure drop

The micro-porous layer (MPL) that covers the surface of the GDL has a significant impact on transport phenomena in GDL-MPL assembly [158]. MPL is typically carbon powder-bound with a hydrophobic agent such as PTFE and has different microstructural properties compared to GDL [158,159]. The smallest length scale of MPL compared to other PEM fuel cell components suggests that MPL has a significant impact on the mass transport overpotentials [160,161]. Different hypotheses have been proposed to describe the role of MPL on the water transport within the cell. Some studies argue that coating a GDL with an MPL facilitates water transport from the catalyst layer to the GDL because of the pore size gradient [55,162,163]. Some studies report that cathode MPL enhances the back diffusion of water from the cathode to anode [13,147,164] and others conclude that the MPL has no impact on the back diffusion of water [165–168].

Blanco et al. [135] studied the effect of MPL in the cathode GDL on the pressure drop measured in the anode and cathode of an operating PEM fuel cell. They measured the two phase flow pressure drop for the anode and cathode when the cell was operating at 25% and 100% relative humidities. Separate experiments were run for the cathode GDL with and without MPL. Fig. 13 shows the variation of cathode and anode pressure drops at different current densities. It can be observed that for current densities above 1000 mA cm^{-2}, the cathode pressure drop of GDL without MPL (25BA) is greater than

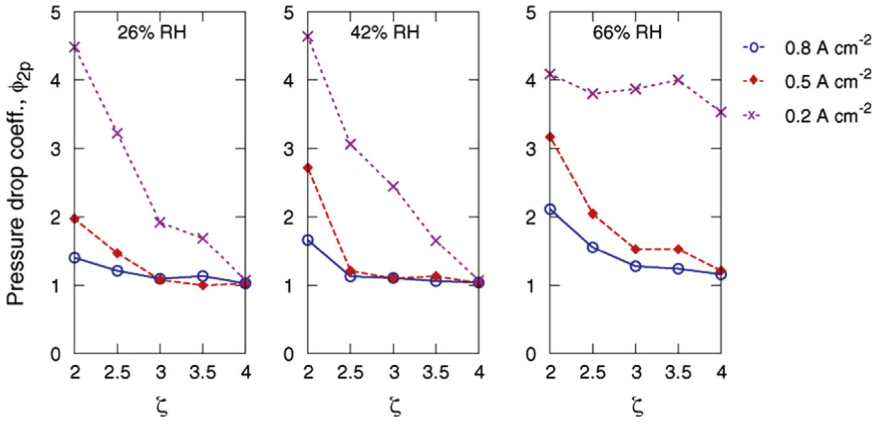

Fig. 12. Effect of the relative humidity on the two-phase flow frictional multiplier reported by Hussaini and Wang [10].

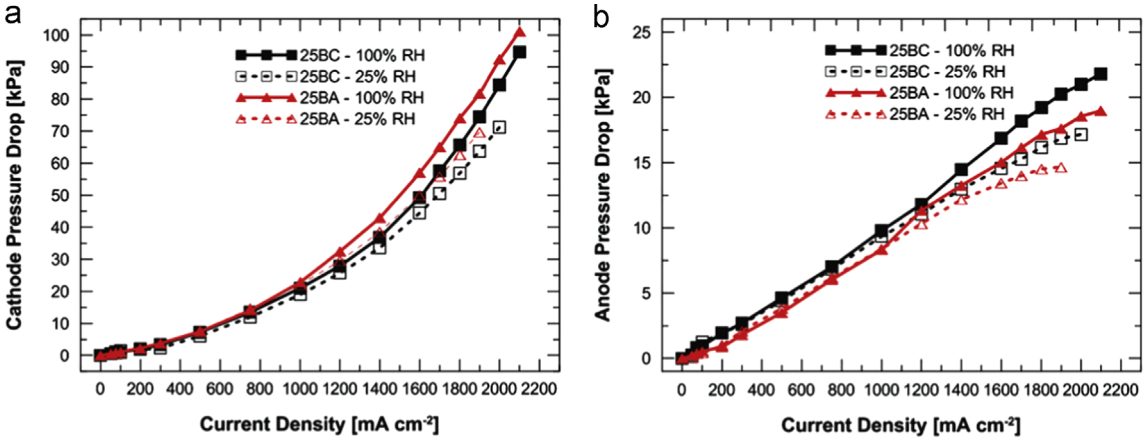

Fig. 13. Effect of MPL on the (a) cathode and (b) anode pressure drop reported by Blanco et al. [135]. 25BA refers to SGL 25BA (GDL without MPL) and 25BC refers to SGL 25BC (GDL with MPL).

the cathode pressure drop for a GDL with MPL (25BC). This has been attributed to a lower amount of accumulated water in the cathode flow channels when MPL was used. In contrast to the cathode in which a GDL without MPL resulted in a higher pressure drop, a GDL without MPL in the anode was observed to cause a lower pressure drop. Such observations can be considered the support of the hypothesis suggesting that MPL impacts water crossover from the cathode to the anode.

4.8. Hysteresis effects in two-phase flow pressure drop

The two-phase flow pressure drop in PEM fuel cell flow channels can exhibit different values when the current density is increasing and then decreasing. This is referred to as pressure drop hysteresis and has been extensively studied by Wilkinson's research group [43,46,49,52,119–121]. They have studied the effects of different parameters on the two-phase flow pressure drop hysteresis by conducting both in situ and ex situ experiments. The parameters they studied include channel outlet configuration (vertical or straight-through) [43], the initial water balance condition in the gas channel [43,119], channel inclination angle [52], flow stoichiometry [119–121], GDL characteristics [119,120], temperature [120,121] and inclusion of microporous layer [121].

Although, as a general trend, the pressure drop increases with the superficial gas velocity, it has been reported that the two-phase pressure drop in PEM fuel cell gas channels does not monotonically increase with superficial gas velocity [43,52]. Instead, the variation of pressure drop based on the gas flow rate exhibits a negative slope for a limited range of gas flow rates, as shown in Fig. 14. Such negative slope is reported to correspond to a two-phase flow pattern change from non-uniform distribution to uniform distribution. The pressure drop hysteresis shown in Fig. 14 corresponds to both the vertical and horizontal outlet configurations. The exit is vertical when it is perpendicular to the flow channel.

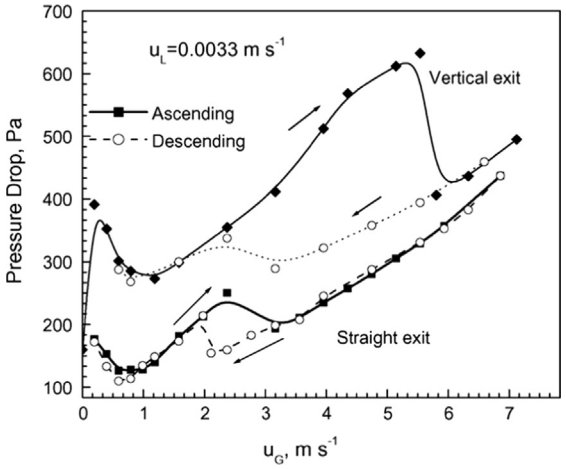

Fig. 14. Pressure drop hysteresis at $j_f = 0.0033$ m s^{-1} reported by Zhang et al. [43].

Fig. 14 shows the pressure drop decreases at superficial gas velocities between 0.2 m s^{-1} and 1.4 m s^{-1} for vertical outlet configuration. Further increase in gas flow rate results in a pressure drop increase and the flow pattern shifts to an even flow distribution. The descending approach shows a lower pressure drop trajectory than the ascending approach. The descending pressure drop trajectory merges with ascending pressure drop trajectory at a superficial gas velocity of 2 m s^{-1}. The figure exhibits a narrower pressure drop hysteresis region for a setup with a straight exit. Furthermore, the negative slope of the pressure drop, which has been known as a sign of transition from non-uniform flow into uniform flow, occurs at a lower pressure for the channel with a straight exit.

The hysteresis region is reported to shrink by increasing the superficial liquid velocity [43,52]. However, the transition pressure drop, defined as the pressure drop at which the flow pattern changes from non-uniform to uniform distribution, remains unchanged for different superficial liquid velocities [43,52].

Zhang et al. [52] studied the effect of channel inclination angle on the two-phase flow pressure drop hysteresis and observed that the pressure drop increases with the inclination angle, as shown in Fig. 15. They tested both positive (upward) and negative (downward) angles and noticed that the pressure drop shows hysteresis effects for upward channels while the hysteresis disappears in downward channels.

In Section 4.4, the effect of flow stoichiometry on two-phase pressure drop was discussed. The flow stoichiometry also affects the hysteresis zone [119,121]. As shown in Fig. 9, increasing the stoichiometry narrows the hysteresis region of the pressure drop. The hysteresis region is large for low stoichiometries of 1–4. This is because the low gas flow is not capable of removing accumulated water, and therefore, there is a significant difference in the amount of water within the gas channel in ascending and descending approaches. The hysteresis seems to disappear for the flow stoichiometry of 5 in Fig. 9. The stoichiometry ratio of 5 is high enough to remove the accumulated liquid water convectively and leave a comparable ascending and descending pressure drop.

MPL also seems to impact the pressure drop hysteresis. Ex situ studies have shown that the inclusion of an MPL does not affect the descending pressure drop while it increases the ascending pressure drop [119]. It has been argued that the GDL with MPL reduces the cross-sectional area of the channel, and therefore, the pressure drop

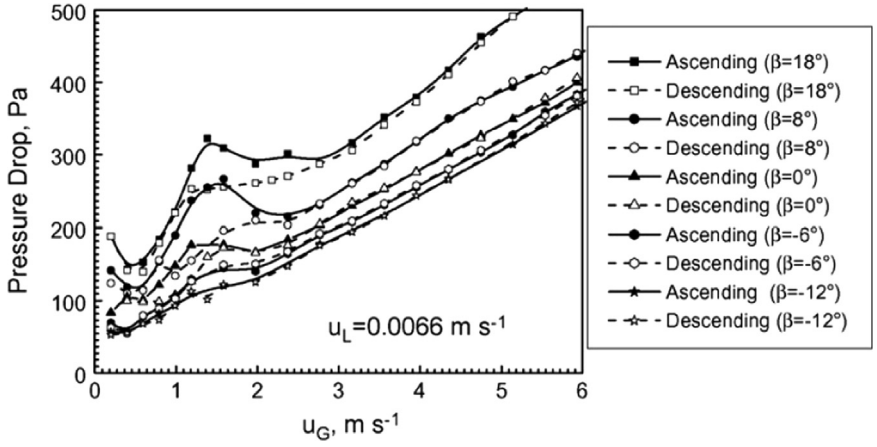

Fig. 15. Effect of the channel inclination angle, β, on the two-phase flow pressure drop hysteresis reported by Zhang et al. [52].

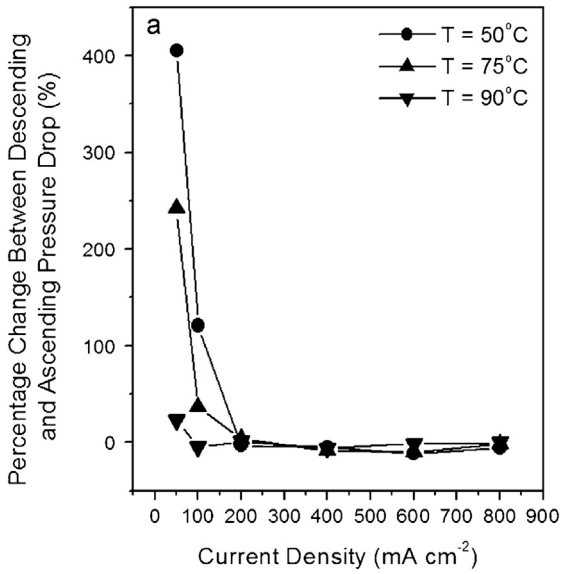

Fig. 16. Effect of temperature on the pressure drop hysteresis reported by Anderson et al. [121].

increases. The inclusion of the MPL in GDL is also reported to increase the simulated current density at which the pressure drop hysteresis initiates [119]. The in situ studies, however, report no clear effect of the MPL on the pressure drop hysteresis except for current densities less than 200 mA cm^{-2} [121].

The other parameter that can affect the pressure drop hysteresis is the initial water balance in the gas channel. For an initially dry gas channel, the ascending pressure drop is lower than the descending pressure drop. However, the excess water in an initially flooded channel causes a higher ascending pressure drop compared to the descending pressure drop. Also, since some portion of water is removed during the ascending approach, the descending pressure drop will be lower than the ascending pressure drop [119].

The effect of the temperature on the pressure drop hysteresis is studied by Anderson et al. [120,121], with the results shown in Fig. 16. It can be observed from the figure that the pressure drop hysteresis decreases as the temperature increases. The lower pressure drop hysteresis for elevated temperatures originates from an increased water removal capacity of the supplied gas.

5. Two-phase flow pressure drop models for the application of PEM fuel cell

The single phase internal flow is very well understood in terms of predicting the flow properties such as the pressure drop. The complicated physics behind the two-phase flow, however, has made it difficult to predict the two-phase flow pressure drop. While enormous effort has been expended in predicting the two-phase pressure drop in large scale industrial applications, there are few works focusing on the two-phase flow pressure drop in minichannels. The two-phase flow in PEM fuel cell minichannels is also different from other industrial applications. This is because of the unique water production and introduction as well as different surface energies of the surrounding walls in PEM fuel cell flow channels. These add to the complication of taking an analytical approach to study the subject of the two-phase flow pressure drop in PEM fuel cell flow channels. In this section, the two-phase flow pressure drop models that have been proposed for the application of PEM fuel cell will be reviewed.

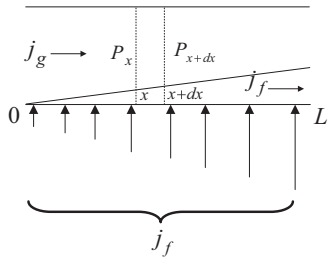

Fig. 17. Water introduction model considered by Zhang et al. [46].

As one of the early stage studies done on the two-phase flow pressure drop in PEM fuel cells, English and Kandlikar [63] extended the Mishima and Hibiki model (Eqs. (15) and (16)) by replacing the turbulent liquid–turbulent gas Chisholm parameter, 21, with a laminar liquid–laminar gas Chisholm parameter, 5. They proposed a modified Chisholm equation that was claimed to result in a better two-phase flow pressure drop prediction:

$$C = 5(1 - e^{-0.319 D_h}) \tag{17}$$

Zhang et al. [49] noticed that the pressure drop predicted by the homogeneous and separated flow models result in large deviations from the actual pressure drop, especially at low mass fluxes of PEM fuel cells. They proposed a flow pattern-dependent pressure drop model that is capable of predicting the two-phase pressure drop hysteresis in parallel channels.

In both of the studies mentioned above, the liquid water is directly introduced into a gas channel with all walls from the same material. Zhang et al. [46] focused on liquid–gas two-phase flow in minichannels with GDL as one of the walls. They compared the measured pressure drop with those predicted by the separated flow model and noticed a significant deviation between the results. This led them to modify the Lockhart–Martinelli (LM) method by considering a gradually increasing water flow rate along the gas channel, as shown in Fig. 17.

They assumed that the pressure drop over a small interval follows the LM method. They defined the Martinelli parameter, χ^2, based on the local superficial liquid velocity, $j_{f|x}$, which has been obtained by modeling the water transport through the porous GDL based on Darcy's law

$$P_x - P_{x+dx} = \phi_g^2 \Delta P_g \, dx = (1 + C\chi + \chi^2)_x \Delta P_g \, dx \tag{18}$$

$$\chi^2{}_{|x} = \frac{j_{f|x}\mu_f}{j_g \mu_g} \tag{19}$$

Substituting Eq. (19) into Eq. (18) yields

$$\frac{dP}{dx} = \Delta P_g \left(1 + C \left(\frac{j_{f|x}\mu_f}{j_g \mu_g} \right)^{0.5} + \frac{j_{f|x}\mu_f}{j_g \mu_g} \right) \tag{20}$$

The total pressure drop was then obtained by integrating Eq. (20) from $x=0$ to $x=L$. The integration was performed with the assumption of uniform and non-uniform liquid water introduction. For uniform water introduction assumption, the integration of Eq. (20) yields

$$\Delta P_{TP} = \Delta P_g (1 + 2/3 C\chi + 1/2\chi^2) \tag{21}$$

For non-uniform liquid introduction, the integration of Eq. (20) yields

$$\Delta P_{TP} = \Delta P_g (1 + 1/2 C\chi + 1/3\chi^2) \tag{22}$$

Fig. 18 compares the experimental results with the predicted pressure drop that has been calculated based on the model proposed in Ref. [46]. The Chisholm parameter of 1.99 in the figure was calculated along with Eq. (16) by using the square

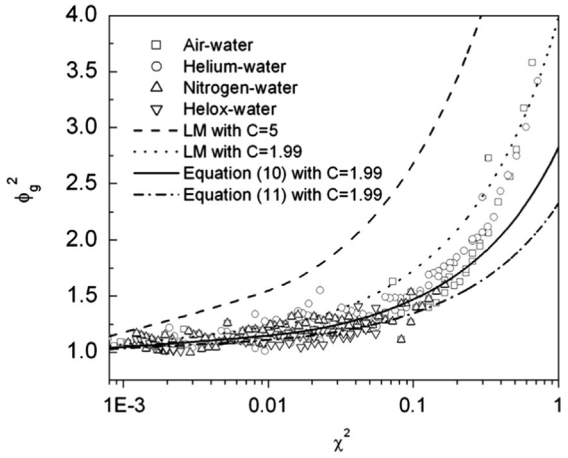

Fig. 18. Comparison of the two-phase flow pressure drop model proposed by Zhang et al. [46] with experimentally measured two-phase flow pressure drop. Line tagging with Eq. (10) corresponds to uniform liquid water introduction which is given by Eq. (21) in the current review. Also line tagging with Eq. (11) corresponds to non-uniform liquid water introduction which is given by Eq. (22) in the current review.

channel size of 1.59 mm. The legends referring to Eqs. (10) and (11) on the figure can be replaced with Eqs. (21) and (22) of the current study, respectively. Fig. 18 shows an overestimated two-phase pressure drop presented by the LM method with $C=5$ and $C=1.99$. Also, different assumptions of uniform and non-uniform liquid water introduction do not exhibit any major differences. Fig. 18 shows that the LM approach is not an appropriate method for predicting the pressure drop for slug flow that corresponds to high ϕ^2. Nevertheless, the pressure drop model proposed by Zhang et al. [46] presents an improved prediction of the two-phase flow pressure drop.

So far, all of the pressure drop models proposed were based on ex situ observations. Anderson et al. [121] conducted in situ experiments and compared the pressure drop measured with the pressure drop predicted based on the correlation given by Zhang et al. [46]. It was observed that the model proposed in Ref. [46] had a closer prediction to the actual pressure drop rather than the classical LM method. However, the proposed model proved to be inferior in expressing all of the water transport phenomena within an operating PEM fuel cell.

Grimm et al. [47] studied the two-phase flow pressure drop at different flow patterns of slug flow, film flow, and mist flow. For slug flow and film flow, they proposed two different series of C equations. In one equation, they proposed a modified C equation by back calculating the measured pressure drop based on Eq. (17). Their proposed C equation is

$$C = A\left(\frac{1-x}{x}\right)^{b} \tag{23}$$

where A and b are given by

$$A = 0.0856(j_f)^{-1.202} \tag{24}$$

$$b = 0.004(j_f)^{-0.526} \tag{25}$$

It was claimed that this correlation yields a mean error of 14%. They also proposed other series of correlations based on the model developed by Lee and Lee [109] by weighting each of the terms in the original correlation and adding the liquid-to-air quality ratio, $(1-x)/x$. For slug flow they proposed:

$$C = 1.9087 Re_f^{-0.405} \lambda^{-0.134} \psi^{-0.421} \left(\frac{1-x}{x}\right)^{-0.107} \tag{26}$$

For film flow they proposed:

$$C = 0.772 Re_f^{0.051} \lambda^{0.016} \psi^{-1.716} \left(\frac{1-x}{x}\right)^{0.034} \tag{27}$$

where λ and ψ are defined by Lee and Lee [109] in Table 4.

The mean error reported by these correlations was 14% for slug flow and 4% for film flow. For mist flow, they suggested using the homogeneous flow model proposed by Dukler [91].

The two-phase flow pressure drop models developed for the application of PEM fuel cells were reviewed in this section. A comparison between the early studies to those done recently reveals some improvements in the models proposed. The experimental setups have been improved and more precise assumptions have been employed for analyzing the results. However, the complicated multiphysics behind the two-phase flow pressure drop seeks further attention in this area. The assumptions need some corrections to yield models with a better prediction of the two-phase flow. In Section 5, the areas that need further attention are introduced.

6. Conclusions

Liquid–gas two-phase flow pressure drop with the application of PEM fuel cells is reviewed in this study. Most of the literature studying the pressure drop in PEM fuel cells is based on parametric studies. These studies compare the pressure drop measured at different liquid and gas flow rates, channel geometries, flow field geometries, gas stoichiometries, surface energies, temperatures, and relative humidities, and try to fit the results with models. Pressure drop in PEM fuel cell gas channels is considered to be a diagnostic tool that describes the amount of liquid water in the gas channels. By monitoring the pressure drop both in the cathode and anode of an operating fuel cell, water transport between the two electrodes can also be identified. Few studies propose modified models that predict the two-phase flow pressure drop in PEM fuel cell gas channels. While in most cases the proposed models are limited to a modified Chisholm parameter, there are some studies that go beyond this and introduce more accurate assumptions to model the unknown parameters. To summarize, the Lockhart–Martinelli (LM) method is an appropriate method to base the pressure drop prediction of slug flow and film flow, while the pressure drop of mist flow is better predicted with the homogeneous flow model because of the comparable liquid and gas superficial velocities.

The two-phase flow pressure drop prediction can be improved by enhancing the current assumptions or experimental conditions. The pressure drop correlations proposed are only applicable over a limited range of working conditions and in most cases are only valid for the experimental setup used in the study. Also, the proposed models are based on the experimental results obtained from ex situ setups with either a single gas channel or parallel gas channels. However, because the pressure drop strongly depends on the flow field geometry, the variation of pressure drop in common flow fields should also be studied. While the pressure drop has been known to depend on the existence of the GDL in the experimental setup, most of the proposed correlations are based on the observation of channels without a GDL.

The pressure drop correlations proposed are based on ex situ experiments. Although ex situ approach may be more accurate when studying a particular phenomenon, the applicability of the findings to an operating fuel cell is in doubt. The electrochemical reactions consume the reactants along the gas channel, and therefore, the gas flow rate differs from the channel inlet to the outlet of an operating cell. Ex situ setup also mimics a constant water introduction along the gas channel, while the water production rate is not uniform along the gas channel of an operating cell. Furthermore, water back diffusion from the cathode to anode is always ignored in ex situ studies. It is of extreme importance to consider all of the multiphysics occurring in an operating cell when studying the topic of two-phase

flow pressure drop. Otherwise, any incomplete assumption may lead to an inaccurate pressure drop model. For instance, the assumption of liquid water being removed as the consequence of the pressure gradient before and after the slug may not be extended to a general scenario. This is because liquid water may be removed by other mechanisms, such as evaporation and/or capillary flow along the channel walls. Similarly, the local superficial water velocity should be determined with a more precise assumption. The water transport through the porous GDL can be modeled by Darcy's law, but the assumption of water being transported at an equal superficial gas velocity does not seem accurate. This is because liquid water detachment from the surface of the GDL depends on different parameters such as GDL surface energy and superficial gas velocity. These reflect the need for a more fundamental study of the two-phase flow pressure drop in PEM fuel cell gas channels.

Acknowledgement

Michigan Technological University is gratefully acknowledged for providing the startup fund for this study.

References

[1] Appleby AJ. Issues in fuel cell commercialization. J Power Sources 1996;58 (2):153–76.
[2] Faghri A, Guo Z. Challenges and opportunities of thermal management issues related to fuel cell technology and modeling. Int J Heat Mass Transf 2005;48 (19):3891–920.
[3] Park GG, Sohn YJ, Yang TH, Yoon YG, Lee WY, Kim CS. Effect of PTFE contents in the gas diffusion media on the performance of PEMFC. J Power Sources 2004;131:182–7.
[4] Ihonen J, Mikkola M, Lindbergh G. Flooding of gas diffusion backing in PEFCs, physical and electrochemical characterization. J Electrochem Soc 2004;151 (8):A1152–61.
[5] Pasaogullari U, Wang CY. Liquid water transport in gas diffusion layer of polymer electrolyte fuel cells. J Electrochem Soc 2004;151:A399–406.
[6] Bazylak A, Sinton D, Djilali N. Dynamic water transport and droplet emergence in PEMFC gas diffusion layers. J Power Sources 2008;176(1):240–6.
[7] Zhang FY, Yang XG, Wang CY. Liquid water removal from a polymer electrolyte fuel cell. J Electrochem Soc 2006;153:A225.
[8] Liu X, Guo H, Ma C. Water flooding and two-phase flow in cathode channels of proton exchange membrane fuel cells. J Power Sources 2006;156(2):267–80.
[9] Li H, Tang Y, Wang Z, Shi Z, Wu S, Song D, et al. A review of water flooding issues in the proton exchange membrane fuel cell. J Power Sources 2008;178 (1):103–17.
[10] Hussaini IS, Wang CY. Visualization and quantification of cathode channel flooding in pem fuel cells. J Power Sources 2009;187(2):444–51.
[11] Mortazavi M, Tajiri K. Effect of the PTFE content in the gas diffusion layer on water transport in polymer electrolyte fuel cells (PEFCs). J Power Sources 2014;245:236–44.
[12] Tüber K, Pócza D, Hebling C. Visualization of water buildup in the cathode of a transparent PEM fuel cell. J Power Sources 2003;124(2):403–14.
[13] Spernjak D, Prasad AK, Advani SG. Experimental investigation of liquid water formation and transport in a transparent single-serpentine PEM fuel cell. J Power Sources 2007;170:334–44.
[14] Kumbur EC, Sharp KV, Mench MM. Liquid droplet behavior and instability in a polymer electrolyte fuel cell flow channel. J Power Sources 2006;161 (1):333–45.
[15] Yang XG, Zhang FY, Lubawy AL, Wang CY. Visualization of liquid water transport in a PEFC. Electrochem Solid State Lett 2004;7:A408.
[16] Owejan JP, Trabold TA, Jacobson DL, Arif M, Kandlikar SG. Effects of flowfield and diffusion layer properties on water accumulation in a PEM fuel cell. Int J Hydrog Energy 2007;32(17):4489–502.
[17] Hickner MA, Siegel NP, Chen KS, Hussey DS, Jacobson DL, Arif M. In situ high-resolution neutron radiography of cross-sectional liquid water profiles in proton exchange membrane fuel cells. J Electrochem Soc 2008;155:B427.
[18] Sinha PK, Halleck P, Wang CY. Quantification of liquid water saturation in a PEM fuel cell diffusion medium using X-ray microtomography. Electrochem Solid State Lett 2006;9(7):A344–8.
[19] Lee SJ, Lim NY, Kim S, Park GG, Kim CS. X-ray imaging of water distribution in a polymer electrolyte fuel cell. J Power Sources 2008;185(2):867–70.
[20] Mench MM, Dong QL, Wang CY. In situ water distribution measurements in a polymer electrolyte fuel cell. J Power Sources 2003;124(1):90–8.
[21] Yang XG, Burke N, Wang CY, Tajiri K, Shinohara K. Simultaneous measurements of species and current distributions in a pefc under low-humidity operation. J Electrochem Soc 2005;152:A759–66.
[22] Bazylak A. Liquid water visualization in PEM fuel cells: a review. Int J Hydrog Energy 2009;34(9):3845–57.
[23] Anderson R, Zhang L, Ding Y, Blanco M, Bi X, Wilkinson DP. A critical review of two-phase flow in gas flow channels of proton exchange membrane fuel cells. J Power Sources 2010;195(15):4531–53.
[24] Kandlikar SG, Grande WJ. Evolution of microchannel flow passages-thermohydraulic performance and fabrication technology. Heat Transf Eng 2003;24(1):3–17.
[25] Triplett KA, Ghiaasiaan SM, Abdel-Khalik SI, Sadowski DL. Gas–liquid two-phase flow in microchannels. Part I: two-phase flow patterns. Int J Multiphase Flow 1999;25(3):377–94.
[26] Wongwises S, Pipathattakul M. Flow pattern, pressure drop and void fraction of two-phase gas-liquid flow in an inclined narrow annular channel. Exp Therm Fluid Sci 2006;30(4):345–54.
[27] Saisorn S, Wongwises S. Flow pattern, void fraction and pressure drop of two-phase air–water flow in a horizontal circular micro-channel. Exp Therm Fluid Sci 2008;32(3):748–60.
[28] Kawahara A, Chung PM-Y, Kawaji M. Investigation of two-phase flow pattern, void fraction and pressure drop in a microchannel. Int J Multiphase Flow 2002;28(9):1411–35.
[29] Saisorn S, Wongwises S. The effects of channel diameter on flow pattern, void fraction and pressure drop of two-phase air–water flow in circular micro-channels. Exp Therm Fluid Sci 2010;34(4):454–62.
[30] Chung PM-Y, Kawaji M. The effect of channel diameter on adiabatic two-phase flow characteristics in microchannels. Int J Multiphase Flow 2004;30:735–61.
[31] Satitchaicharoen Pongsiri, Wongwises Somchai. Two-phase flow pattern maps for vertical upward gasliquid flow in mini-gap channels. Int J Multiphase Flow 2004;30(2):225–36.
[32] Saisorn S, Wongwises S. An experimental investigation of two-phase air–water flow through a horizontal circular micro-channel. Exp Therm Fluid Sci 2009;33(2):306–15.
[33] Ide Hideo, Matsumura Hirohisa. Frictional pressure drops of two-phase gas–liquid flow in rectangular channels. Exp Therm Fluid Sci 1990;3 (4):362–72.
[34] Wambsganss MW, Jendrzejczyk JA, France DM. Two-phase flow patterns and transitions in a small, horizontal, rectangular channel. Int J Multiphase Flow 1991;17:327–42.
[35] Lowry B, Kawaji M. Adiabatic vertical two-phase flow in narrow flow channels. AIChE Symp Ser 1988;84:133–9.
[36] Venkatesan M, Das Sarit K, Balakrishnan AR. Effect of diameter on two-phase pressure drop in narrow tubes. Exp Therm Fluid Sci 2011;35(3):531–41.
[37] Choi CW, Yu DI, Kim MH. Adiabatic two-phase flow in rectangular micro-channels with different aspect ratios: part I – flow pattern, pressure drop and void fraction. Int J Heat Mass Transf 2011;54:616–24.
[38] Wang CC, Yang KS, Chang YJ, Lu DC. Characteristics of air–water two-phase flow in a 3-mm smooth tube. Can J Chem Eng 2000;78(5):1011–6.
[39] Xu JL, Cheng P, Zhao TS. Gas–liquid two-phase flow regimes in rectangular channels with mini/micro gaps. Int J Multiphase Flow 1999;25(3):411–32.
[40] Pettersen J. Flow vaporization of co2 in microchannel tubes. Exp Therm Fluid Sci 2004;28:111–21.
[41] Zhao TS, Bi QC. Co-current air–water two-phase flow patterns in vertical triangular microchannels. Int J Multiphase Flow 2001;27(5):765–82.
[42] Triplett KA, Ghiaasiaan SM, Abdel-Khalik SI, LeMouel A, McCord BN. Gas liquid two-phase flow in microchannels: part II: void fraction and pressure drop. Int J Multiphase Flow 1999;25:395–410.
[43] Zhang L, Bi HT, Wilkinson DP, Stumper J, Wang H. Gas–liquid two-phase flow patterns in parallel channels for fuel cells. J Power Sources 2008;183 (2):643–50.
[44] Lu Z, Kandlikar SG, Rath C, Grimm M, Domigan W, White AD, et al. Water management studies in PEM fuel cells, part II: ex situ investigation of flow maldistribution, pressure drop and two-phase flow pattern in gas channels. Int J Hydrog Energy 2009;34(8):3445–56.
[45] Lu Z, Rath C, Zhang G, Kandlikar SG. Water management studies in PEM fuel cells, part IV: effects of channel surface wettability, geometry and orientation on the two-phase flow in parallel gas channels. Int J Hydrog Energy 2011;36 (16):9864–75.
[46] Zhang L, Bi XT, Wilkinson DP, Anderson R, Stumper J, Wang H. Gas–liquid two-phase flow behavior in minichannels bounded with a permeable wall. Chem Eng Sci 2011;66(14):3377–85.
[47] Grimm M, See EJ, Kandlikar SG. Modeling gas flow in PEMFC channels: part I —flow pattern transitions and pressure drop in a simulated ex situ channel with uniform water injection through the GDL. Int J Hydrog Energy 2012;37:12489–503.
[48] Wu TC, Djilali N. Experimental investigation of water droplet emergence in a model polymer electrolyte membrane fuel cell microchannel. J Power Sources 2012;208:248–56.
[49] Zhang L, Bi HT, Wilkinson DP, Stumper J, Wang H. Gas flow rate distributions in parallel minichannels for polymer electrolyte membrane fuel cells: experiments and theoretical analysis. J Power Sources 2010;195(10):3231–9.
[50] Knights SD, Colbow KM, Pierre JS, Wilkinson DP. Aging mechanisms and lifetime of PEFC and DMFC. J Power Sources 2004;127:127–34.
[51] Trabold Thomas A. Minichannels in polymer electrolyte membrane fuel cells. Heat Transf Eng 2005;26(3):3–12.
[52] Zhang L, Du W, Bi HT, Wilkinson DP, Stumper J, Wang H. Gas–liquid two-phase flow distributions in parallel channels for fuel cells. J Power Sources 2009;189(2):1023–31.

[53] Chen J. Experimental study on the two phase flow behavior in PEM fuel cell parallel channels with porous media inserts. J Power Sources 2010;195(4):1122–9.
[54] Kandlikar SG, Lu Z, Domigan WE, White AD, Benedict MW. Measurement of flow maldistribution in parallel channels and its application to ex-situ and in-situ experiments in pemfc water management studies. Int J Heat Mass Transf 2009;52:1741–52.
[55] Nam JH, Kaviany M. Effective diffusivity and water-saturation distribution in single-and two-layer PEMFC diffusion medium. Int J Heat Mass Transf 2003;46(24):4595–611.
[56] Benziger J, Nehlsen J, Blackwell D, Brennan T, Itescu J. Water flow in the gas diffusion layer of PEM fuel cells. J Membr Sci 2005;261(1–2):98–106.
[57] Litster S, Sinton D, Djilali N. Ex situ visualization of liquid water transport in PEM fuel cell gas diffusion layers. J Power Sources 2006;154(1):95–105.
[58] Tamayol A, Bahrami M. Water permeation through gas diffusion layers of proton exchange membrane fuel cells. J Power Sources 2011:6356–61.
[59] Manke I, Hartnig Ch, Grünerbel M, Lehnert W, Kardjilov N, Haibel A, et al. Investigation of water evolution and transport in fuel cells with high resolution synchrotron x-ray radiography. Appl Phys Lett 2007;90(17):174105.
[60] Kariyasaki A, Fukano T, Ousaka A, Kagawa M. Characterization of time-varying void fraction in isothermal air–water co-current flow in horizontal capillary tube. Trans JSME 1991:4036–43.
[61] Zivi SM. Estimation of steady-state steam void-fraction by means of the principle of minimum entropy production. J Heat Transf AMSE 1964;86:247–52.
[62] Choi KI, Pamitran AS, Oh CY, Oh JT. Two-phase pressure drop of R-410A in horizontal smooth minichannels. Int J Refrig 2008;31:119–29.
[63] English NJ, Kandlikar SG. An experimental investigation into the effect of surfactants on air–water two-phase flow in minichannels. Heat Transf Eng 2006;27(4):99–109.
[64] Lockhart RW, Martinelli RC. Proposed correlation of data for isothermal two-phase, two-components flow in pipes. Chem Eng Prog 1949;45:39–48.
[65] Bao ZY, Bosnich MG, Haynes BS. Estimation of void fraction and pressure drop for two-phase flow in fine passages. Chem Eng Res Des 1994;72:625–32.
[66] Chang SD, Ro ST. Pressure drop of pure HFC refrigerants and their mixtures flowing in capillary tubes. Int J Multiphase Flow 1996;22:551–61.
[67] Yan YY, Lin TF. Evaporation heat transfer and pressure drop of refrigerant R-134a in a small pipe. Int J Heat Mass Transf 1998;41(24):4183–94.
[68] Wang CC, Chang SKChiangYJ, Chung TW. Two-phase flow resistance of refrigerants R-22, R-410A and R-407C in small diameter tubes. Chem Eng Res Des 2001;79(5):553–60.
[69] Chen IY, Yang KS, Chang YJ, Wang CC. Two-phase pressure drop of air–water and R-410A in small horizontal tubes. Int J Multiphase Flow 2001;27(7):1293–9.
[70] Zhang M, Webb RL. Correlation of two-phase friction for refrigerants in small-diameter tubes. Exp Therm Fluid Sci 2001;25:131–9.
[71] Yu W, France DM, Wambsganss MW, Hull JR. Two-phase pressure drop, boiling heat transfer, and critical heat flux to water in a small-diameter horizontal tube. Int J Multiphase Flow 2002;28(6):927–41.
[72] Bandarra Filho EP, Saiz Jabardo JM, Barbieri PEL. Convective boiling pressure drop of refrigerant r-134a in horizontal smooth and microfin tubes. Int J Refrig 2004;27(8):895–903.
[73] Greco A, Vanoli GP. Evaporation of refrigerants in a smooth horizontal tube: prediction of R22 and R507 heat transfer coefficients and pressure drop. Appl Therm Eng 2004;24:2189–206.
[74] Wongsa-ngam J, Nualboonrueng T, Wongwises S. Performance of smooth and micro-fin tubes in high mass flux region of R-134a during evaporation. Heat Mass Transf 2004;40:425–35.
[75] Choi K, Pamitran AS. Effect of boiling heat transfer of horizontal smooth minichannel for R-410A and R-407C. J Mech Sci Tech 2005;19:156–63.
[76] Pehlivan K, Hassan I, Vaillancourt M. Experimental study on two-phase flow and pressure drop in millimeter-size channels. Appl Therm Eng 2006;26:1506–14.
[77] Chen IY, Chen YM, Liaw JS, Wang CC. Two-phase frictional pressure drop in small rectangular channels. Exp Therm Fluid Sci 2007;32(1):60–6.
[78] Mauro AW, Moreno JM, Mastrullo R, Thome JR. Comparison of experimental pressure drop data for two phase flows to prediction methods using a general model. Int J Refrig 2007;30(8):1358–67.
[79] Lee CY, Lee SY. Pressure drop of two-phase plug flow in round mini-channels: influence of surface wettability. Exp Therm Fluid Sci 2008;32(8):1716–22.
[80] Tran TN, Chyu MC, Wambsganss MW, France DM. Two-phase pressure drop of refrigerants during flow boiling in small channels: an experimental investigation and correlation development. Int J Multiphase Flow 2000;26(11):1739–54.
[81] da Silva Lima RJ, Quibn JM, Kuhn C, Boyman T, Thome JR. Ammonia two-phase flow in a horizontal smooth tube: flow pattern observations, diabatic and adiabatic frictional pressure drops and assessment of prediction methods. Int J Heat Mass Transf 2009;52:2273–88.
[82] Hu HT, Ding GL, Huang XC, Deng B, Gao YF. Pressure drop during horizontal flow boiling of R410A/oil mixture in 5 mm and 3 mm smooth tubes. Appl Therm Eng 2009;29(16):3353–65.
[83] Kaew-On J, Wongwises S. Experimental investigation of evaporation heat transfer coefficient and pressure drop of R-410A in a multiport mini-channel. Int J Refrig 2009;32(1):124–37.
[84] Quiben JM, Cheng L, da Silva Lima RJ, Thome JR. Flow boiling in horizontal flattened tubes: part I – two-phase frictional pressure drop results and model. Int J Heat Mass Transf 2009;52:3634–44.
[85] Wu J, Koettig T, Franke Ch, Helmer D, Eisel T, Haug F, et al. Investigation of heat transfer and pressure drop of CO2 two-phase flow in a horizontal minichannel. Int J Heat Mass Transf 2011;54:2154–62.
[86] Saisorn Sira, Wongwises Somchai. Two-phase air–water flow in micro-channels: an investigation of the viscosity models for pressure drop prediction. Int Commun Heat Mass 2011;38(2):212–7.
[87] McAdams WH, Woods WK, Heroman LC. Vaporization inside horizontal tubes. Trans ASME 1942;64:193–200.
[88] Akers WW, Deans HA, Crosser OK. Condensing heat transfer within horizontal tubes. Chem Eng Prog 1958;54:89–90.
[89] Cicchitti A, Lombardi C, Silvestri M, Soldaini G, Zavalluilli R. Two-phase cooling experiments-pressure drop, heat transfer and burnout measurements. Energia Nucleare 1960;7:407–25.
[90] Owens WL. Two-phase pressure gradient. Int Dev Heat Transf, Pt. II. New York: ASME; 1961.
[91] Dukler AE, Wicks M, Cleaveland RG. Pressure drop and hold up in two-phase flow. AlChE J 1964;10:38–51.
[92] Beattie DRH, Whalley PB. A simple two-phase frictional pressure drop calculation method. Int J Multiphase Flow 1982;8:83–7.
[93] Lin S, Kwok CCK, Li RY, Chen ZH, Chen ZY. Local frictional pressure drop during vaporization of R-12 through capillary tubes. Int J Multiphase Flow 1991;17:95–102.
[94] Kim SM, Mudawar I. Universal approach to predicting two-phase frictional pressure drop for mini/micro-channel saturated flow boiling. Int J Heat Mass Transf 2013;58:718–34.
[95] Lee J, Mudawar I. Two-phase flow in high-heat-flux micro-channel heat sink for refrigeration cooling applications: part I—pressure drop characteristics. Int J Heat Mass Transf 2005;48(5):928–40.
[96] Saisorn S, Wongwises S. An inspection of viscosity model for homogeneous two-phase flow pressure drop prediction in a horizontal circular micro-channel. Int Commun Heat Mass 2008;35(7):833–8.
[97] Choi Chiwoong, Kim Moohwan. Flow pattern based correlations of two-phase pressure drop in rectangular microchannels. Int J Heat Fluid Flow 2011;32(6):1199–207.
[98] Shah RK, London AL. Laminar flow forced convection in ducts. New York: Academic Press; 1978.
[99] Wang CC, Chiang CS, Lu DC. Visual observation of two-phase flow pattern of R-22, R-134a, and R-407C in a 6.5-mm smooth tube. Exp Therm Fluid Sci 1997;15(4):395–405.
[100] Chisholm D. A theoretical basis for the Lockhart–Martinelli correlation for two-phase flow. Int J Heat Mass Transf 1967;10:1767–78.
[101] Friedel L. Improved friction pressure drop correlations for horizontal and vertical two-phase pipe flow. European two-phase group meeting, Ispra, Italy, Paper E2; 1979.
[102] Müller-Steinhagen H, Heck K. A simple friction pressure drop correlation for two-phase flow in pipes. Chem Eng Process 1986;20(6):297–308.
[103] Sun Licheng, Mishima Kaichiro. Evaluation analysis of prediction methods for two-phase flow pressure drop in mini-channels. Int J Multiphase Flow 2009;35(1):47–54.
[104] Ribatski G, Wojtan L, Thome JR. An analysis of experimental data and prediction methods for two-phase frictional pressure drop and flow boiling heat transfer in micro-scale channels. Exp Therm Fluid Sci 2006;31(1):1–19.
[105] Jung DS, Radermacher R. Prediction of pressure drop during horizontal annular flow boiling of pure and mixed refrigerants. Int J Heat Mass Transf 1989;32:2435–46.
[106] Mishima K, Hibiki T. Some characteristics of air–water two-phase flow in small diameter vertical tubes. Int J Multiphase Flow 1996;22:703–12.
[107] Wambsganss. Frictional pressure gradient in two-phase flow in a small horizontal rectangular channel. Exp Therm Fluid Sci 1992;5:40–56.
[108] Yang C-Y, Webb RL. Friction pressure drop of r-12 in small hydraulic diameter extruded aluminum tubes with and without micro-fins. Int J Heat Mass Trans 1996;39(4):801–9.
[109] Lee HL, Lee SY. Pressure drop correlations for two-phase flow within horizontal rectangular channels with small heights. Int J Multiphase Flow 2001;27:783–96.
[110] Hwang Yun Wook, Kim Min Soo. The pressure drop in microtubes and the correlation development. Int J Heat Mass Transf 2006;49:1804–12.
[111] Li Wei, Wu Zan. A general correlation for adiabatic two-phase pressure drop in micro/mini-channels. Int J Heat Mass Transf 2010;53:2732–9.
[112] Zhang W, Hibiki T, Mishima K. Correlations of two-phase frictional pressure drop and void fraction in mini-channel. Int J Heat Mass Transf 2010;53:453–65.
[113] Li Wei, Wu Zan. Generalized adiabatic pressure drop correlations in evaporative micro/mini-channels. Exp Therm Fluid Sci 2011;35(6):866–72.
[114] Concus P, Finn R. On the behavior of a capillary surface in a wedge. Proc Natl Acad Sci 1969;63:292–9.
[115] Yu Xiao, Pingwen Ming, Ming Hou, Baolian Yi, Shao Zhi-Gang. The critical pressure drop for the purge process in the anode of a fuel cell. J Power Sources 2009;188(1):163–9.
[116] Radhakrishnan Vijay, Haridoss Prathap. Effect of gdl compression on pressure drop and pressure distribution in pemfc flow field. Int J Hydrog Energy 2011;36(22):14823–8.
[117] Allen Jeffrey S. Two phase flow in small channels and the implications for pem fuel cell operation. ECS Trans 2006;3:1197–206.
[118] Hsieh Shou-Shing, Huang Yi-Ji, Her Bing-Shyan. Pressure drop on water accumulation distribution for a micro pem fuel cell with different flow field plates. Int J Heat Mass Transf 2009;52:5657–9.
[119] Anderson R, Wilkinson DP, Bi X, Zhang L. Two-phase flow pressure drop hysteresis in parallel channels of a proton exchange membrane fuel cell. J Power Sources 2010;195(13):4168–76.

[120] Anderson Ryan, Wilkinson David, Bi Xiaotao, Zhang Lifeng. Two-phase flow pressure drop hysteresis under typical operating conditions for a proton exchange membrane fuel cell. ECS Trans 2010;28(30):127–37.
[121] Anderson R, Wilkinson DP, Bi X, Zhang L. Two-phase flow pressure drop hysteresis in an operating proton exchange membrane fuel cell. J Power Sources 2011;196:8031–40.
[122] Rodatz Paul, Bchi Felix, Onder Chris, Guzzella Lino. Operational aspects of a large pefc stack under practical conditions. J Power Sources 2004;128(2):208–17.
[123] Barbir F, Gorgun H, Wang X. Relationship between pressure drop and cell resistance as a diagnostic tool for pem fuel cells. J Power Sources 2005;141:96–101.
[124] Yamada H, Hatanaka T, Murata H, Morimoto Y. Measurement of flooding in gas diffusion layers of polymer electrolyte fuel cells with conventional flow field. J Electrochem Soc 2006;153(9):A1748–54.
[125] Jiao Kui, Alaefour Ibrahim E, Karimi Gholamreza, Li Xianguo. Cold start characteristics of proton exchange membrane fuel cells. Int J Hydrog Energy 2011;36(18):11832–45.
[126] Ma HP, Zhang HM, Hu J, Cai YH, Yi BL. Diagnostic tool to detect liquid water removal in the cathode channels of proton exchange membrane fuel cells. J Power Sources 2006;162(1):469–73.
[127] Ge S, Wang CY. Liquid water formation and transport in the pefc anode. J Electrochem Soc 2007;154(10):B998–1005.
[128] Liu Xuan, Guo Hang, Ye Fang, Ma Chong Fang. Water flooding and pressure drop characteristics in flow channels of proton exchange membrane fuel cells. Electrochim Acta 2007;52(11):3607–14.
[129] Ito Kohei, Ashikaga Kensuke, Masuda Hiromitsu, Oshima Toshihiro, Kakimoto Yasushi, Sasaki Kazunari. Estimation of flooding in pemfc gas diffusion layer by differential pressure measurement. J Power Sources 2008;175(2):732–8.
[130] Spernjak Dusan, Prasad AjayK, Advani Suresh G. In situ comparison of water content and dynamics in parallel, single-serpentine, and interdigitated flow fields of polymer electrolyte membrane fuel cells. J Power Sources 2010;195(11):3553–68.
[131] Kandlikar SG, Lu Z, Lin TY, Cooke D, Daino M. Uneven gas diffusion layer intrusion in gas channel arrays of proton exchange membrane fuel cell and its effects on flow distribution. J Power Sources 2009;194(1):328–37.
[132] Akhtar N, Qureshi A, Scholta J, Hartnig C, Messerschmidt M, Lehnert W. Investigation of water droplet kinetics and optimization of channel geometry for pem fuel cell cathodes. Int J Hydrog Energy 2009;34(7):3104–11.
[133] Chen J. Dominant frequency of pressure drop signal as a novel diagnostic tool for the water removal in proton exchange membrane fuel cell flow channel. J Power Sources 2010;195(4):1177–81.
[134] Dillet J, Lottin O, Maranzana G, Didierjean S, Conteau D, Bonnet C. Direct observation of the two-phase flow in the air channel of a proton exchange membrane fuel cell and of the effects of a clogging/unclogging sequence on the current density distribution. J Power Sources 2010;195(9):2795–9.
[135] Blanco M, Wilkinson DP, Wang H. Application of water barrier layers in a proton exchange membrane fuel cell for improved water management at low humidity conditions. Int J Hydrogen Energy 2011;36:3635–48.
[136] Colosqui CE, Cheah MJ, Kevrekidis IG, Benziger JB. Droplet and slug formation in polymer electrolyte membrane fuel cell flow channels: the role of interfacial forces. J Power Sources 2011;196(23):10057–68.
[137] Li Xianguo, Sabir Imran, Park Jaewan. A flow channel design procedure for pem fuel cells with effective water removal. J Power Sources 2007;163(2):933–42.
[138] Taccani Rodolfo, Zuliani Nicola. Effect of flow field design on performances of high temperature pem fuel cells: experimental analysis. Int J Hydrog Energy 2011;36(16):10282–7.
[139] Bachman J, Charvet M, Santamaria A, Tang HY, Park JW, Walker R. Experimental investigation of the effect of channel length on performance and water accumulation in a PEMFC parallel flow field. Int J Hydrog Energy 2012;37(22):17172–9.
[140] Hsieh Shou-Shing, Her Bing-Shyan, Huang Yi-Ji. Effect of pressure drop in different flow fields on water accumulation and current distribution for a micro pem fuel cell. Energy Convers Manag 2011;52(2):975–82.
[141] Li Xianguo, Sabir Imran. Review of bipolar plates in PEM fuel cells: flow-field designs. Int J Hydrog Energy 2005;30(4):359–71.
[142] Barbir Frano. PEM fuel cells: theory and practice. Access Online via Elsevier; 2012.
[143] Li Xianguo. Principles of fuel cells. Taylor & Francis; 2006.
[144] Nguyen TV, He W. Handbook of fuel cells. John Wiley & Sons Ltd.; 2003.
[145] Rath Cody D, Kandlikar Satish G. Liquid filling in a corner with a fibrous wall an application to two-phase flow in pem fuel cell gas channels. Colloids Surf A: Physicochem Eng Aspects 2011;384(1):653–60.
[146] Weng FB, Su A, Hsu CY. The study of the effect of gas stoichiometric flow rate on the channel flooding and performance in a transparent fuel cell. Int J Hydrog Energy 2007;32(6):666–76.
[147] Lin G, Nguyen TV. Effect of thickness and hydrophobic polymer content of the gas diffusion layer on electrode flooding level in a PEMFC. J Electrochem Soc 2005;152:A1942–8.
[148] Ous T, Arcoumanis C. Visualisation of water accumulation in the flow channels of pemfc under various operating conditions. J Power Sources 2009;187(1):182–9.
[149] Hickner MA, Siegel NP, Chen KS, McBrayer DN, Hussey DS, Jacobson DL, et al. Real-time imaging of liquid water in an operating proton exchange membrane fuel cell. J Electrochem Soc 2006;153:A902.
[150] Owejan JP, Gagliardo JJ, Sergi JM, Kandlikar SG, Trabold TA. Water management studies in pem fuel cells, part i: fuel cell design and in situ water distributions. Int J Hydrog Energy 2009;34(8):3436–44.
[151] Liu X, Guo H, Ye F, Ma CF. Flow dynamic characteristics in flow field of proton exchange membrane fuel cells. Int J Hydrog Energy 2008;33(3):1040–51.
[152] Zhan Zhigang, Wang Chen, Fu Weiguo, Pan Mu. Visualization of water transport in a transparent pemfc. Int J Hydrog Energy 2012;37(1):1094–105.
[153] Paquin Mathieu, Fréchette Luc G. Understanding cathode flooding and dry-out for water management in air breathing pem fuel cells. J Power Sources 2008;180(1):440–51.
[154] Yan Wei-Mon, Wang Xiao-Dong, Mei Sen-Sin, Peng Xiao-Feng, Guo Yi-Fan, Su Ay. Effects of operating temperatures on performance and pressure drops for a 256cm2 proton exchange membrane fuel cell: an experimental study. J Power Sources 2008;185(2):1040–8.
[155] Lim C, Wang CY. Effects of hydrophobic polymer content in GDL on power performance of a PEM fuel cell. Electrochim Acta 2004;49(24):4149–56.
[156] Xu H, Song Y, Kunz HR, Fenton JM. Effect of elevated temperature and reduced relative humidity on orr kinetics for pem fuel cells. J Electrochem Soc 2005;152:A1828.
[157] Neyerlin KC, Gasteiger HA, Mittelsteadt CK, Jorne J, Gu W. Effect of relative humidity on oxygen reduction kinetics in a pemfc. J Electrochem Soc 2005;152:A1073.
[158] Wargo EA, Schulz VP, Çeçen A, Kalidindi SR, Kumbur EC. Resolving macro- and micro-porous layer interaction in polymer electrolyte fuel cells using focused ion beam and x-ray computed tomography. Electrochim Acta 2012;87:201–12.
[159] Parikh N, Allen JS, Yassar RS. Microstructure of gas diffusion layers for PEM fuel cells. Fuel Cells 2012;12.
[160] Litster S, McLean G. PEM fuel cell electrodes. J Power Sources 2004;130:61–76.
[161] Baranov IE, Grigoriev SA, Ylitalo D, Fateev VN, Nikolaev II. Transfer processes in PEM fuel cell: influence of electrode structure. Int J Hydrog Energy 2006;31(2):203–10.
[162] Pasaogullari U, Wang CY, Chen KS. Two-phase transport in polymer electrolyte fuel cells with bilayer cathode gas diffusion media. J Electrochem Soc 2005;152(8):A1574–82.
[163] Pasaogullari U, Wang CY. Two-phase transport and the role of micro-porous layer in polymer electrolyte fuel cells. Electrochim Acta 2004;49(25):4359–69.
[164] Weber AZ, Newman J. Effects of microporous layers in polymer electrolyte fuel cells. J Electrochem Soc 2005;152:A677.
[165] Pharoah Jon G, Peppley Brant, Atiyeh Hasan, Halliop Ela, Karan Kunal, Phoenix Aaron. Investigating the role of a microporous layer on the water transport and performance of a PEMFC. ECS Trans 2006;3(1):1227–37.
[166] Karan K, Atiyeh H, Phoenix A, Halliop E, Pharoah J, Peppley B. An experimental investigation of water transport in pemfcs. Electrochem Solid-State Lett 2007;10:B34.
[167] Atiyeh HK, Karan K, Peppley B, Phoenix A, Halliop E, Pharoah J. Experimental investigation of the role of a microporous layer on the water transport and performance of a pem fuel cell. J Power Sources 2007;170(1):111–21.
[168] Malevich Dzmitry, Halliop Ela, Peppley Brant A, Pharoah Jon G, Karan Kunal. Investigation of charge-transfer and mass-transport resistances in pemfcs with microporous layer using electrochemical impedance spectroscopy. J Electrochem Soc 2009;156(2):B216–24.